RSC Advances

This is an *Accepted Manuscript*, which has been through the Royal Society of Chemistry peer review process and has been accepted for publication.

Accepted Manuscripts are published online shortly after acceptance, before technical editing, formatting and proof reading. Using this free service, authors can make their results available to the community, in citable form, before we publish the edited article. This *Accepted Manuscript* will be replaced by the edited, formatted and paginated article as soon as this is available.

You can find more information about *Accepted Manuscripts* in the Information for Authors.

Please note that technical editing may introduce minor changes to the text and/or graphics, which may alter content. The journal's standard Terms & Conditions and the Ethical guidelines still apply. In no event shall the Royal Society of Chemistry be held responsible for any errors or omissions in this *Accepted Manuscript* or any consequences arising from the use of any information it contains.

ROYAL SOCIETY OF CHEMISTRY

www.rsc.org/advances

Measuring methods for thermoelectric propriety of one-dimensional nanostructural materials

Yang Liu, Mingliang Zhang*, An Ji, Fuhua Yang, and Xiaodong Wang*

Engineering Research Center for Semiconductor Integrated Technology, Institute of Semiconductors, Chinese Academy of Sciences, Beijing 100083, China. E-mail:xdwang@semi.ac.cn, zhangml@semi.ac.cn; Fax:+86-10-82305141

Thermoelectric materials and devices have attracted extensive research interests. Great progress has been obtained in improving the thermoelectric figure of merit ZT of several one-dimensional (1D) nanostructural materials. Simultaneously, tremendous efforts were devoted to characterize thermoelectric performance of nanostructural materials and associated devices. Accurate measurements of Seebeck coefficient and thermal conductivity of 1D nanostructural materials were still stiff task. This review explored the latest research results on measuring methods for thermoelectric properties of 1D nanostructural materials. Five frequently used methods to measure Seebeck coefficient would be presented. Twelve kinds of popular methods to measure thermal conductivity would be described. Device structures, measuring principles, merits and shortages, and application examples of every method would be discussed in details. Two potential hot topics in measuring thermoelectric properties of 1D nanostructural materials would be proposed.

I Introduction

One of the great challenges of modern society is the energy crisis, including energy storage, consumption, and dissipation. Consequently, functional materials and devices, having the ability to reduce power dissipation routes, have attracted enormous interests.[1-4] Among these, thermoelectric materials, which could direct transform thermal and electrical energy in solid-state based on Seebeck and Peltier effects,[5] hold great promise for improving energy conversion and harvesting.[6,7] These materials could be associated with solar system,[8-10] sensors[11] and etc..[12-14] For example, the performances of ever-shrinking electronic chips were historically enhanced by increasing power and increasing on-chip power density. Heat generation from the chips, however, was spatially non-uniform, resulting in regions of localized high heat fluxes known as hotspots (>1000 W/cm^2) which presented a cooling challenge.[13] The localized, on-chip, solid-state thermoelectric refrigeration was expected to open up the possibility of microelectronic chips with efficient thermal control. However, there was only modest progress for several years because of the real challenges faced by researchers trying to enhance the thermoelectric performance. Fortunately, low dimensional nanostructures, compared with their bulk counterparts, have been proposed to have better thermoelectric performance due to increased phonon scattering and quantum confinement in the early 1990s by Hicks et al..[15] Later, several 1D nanostructures, such as nanowires (NWs),[16-18] nanotubes (NTs),[19-21] have been extensively investigated. Up to now, a tremendous amount of work was committed to manufacture 1D materials and characterize their thermoelectric performance.[22-31] Nevertheless, the measuring methods for thermoelectric properties of 1D nanostructure materials were still key issues to obtain materials with improved thermoelectric performance.

RSC Advances Accepted Manuscript

I-1 Principles of thermoelectricity

The thermoelectric effect was fundamentally a direct solid-state conversion of between thermal and electrical energy by Seebeck and Peltier effects. For conducting or semiconducting materials, the microscopic mechanism of the Seebeck effect mostly depended on the carriers distribution under a temperature gradient. The carriers (electrons or holes) were uniformly distributed without the temperature gradient. However, once the temperature gradient existed, the carriers at the hot end hosted larger kinetic energy and tended to diffuse to the cold end. As a consequence of the charge carrier diffusion, the accumulation of the electric charge established an internal electric field to prevent the further diffusion of the carriers. In the end, the diffusion caused by the temperature gradient and the drift of carriers caused by the internal electric field reached their dynamic equilibrium. Consequently, the Seebeck potential between the hot and cold extremity of the material was established.

In order to quantify the Seebeck effect of various materials, Seebeck coefficient/thermoelectric power (TEP) was defined as the ratio between the thermoelectric induced voltage and the temperature difference across the material. That was

$$S = -\frac{\Delta V}{\Delta T} \qquad (1\text{-}1)$$

where ΔT, ΔV are the temperature difference along the NW and the thermoelectric voltage induced by temperature difference, respectively. The sign depended on characteristics of materials: positive for p-type semiconductor and minus for n-type semiconductor.

As for the performance of a thermoelectric material, it was tightly correlated with its electronic and phononic transportion characterization and was normally described by the dimensionless thermoelectric figure of merit,[32,33]

$$\mathrm{ZT} = \frac{S^2 \sigma T}{\kappa} \qquad (1\text{-}2)$$

where T represents the environmental temperature of a working device, S, σ, k are the Seebeck coefficient, electrical conductivity, and thermal conductivity of the thermoelectric material, respectively. From the equation (1-2), a large power factor, $S^2\sigma$, implied that the material could output large voltage or current, and a material with low heat conductivity possessed high ZT.

I-2 ZT of 1D nanostructural materials

To enhance the performance of thermoelectric materials, a great effort had been made to reduce their electrical conductivities and increase the Seebeck coefficients. For example, doping had been proved to be a promising approach to improve ZT of nanoscale materials because of its remarkable impact on thermoelectric properties of nanomaterials.[34-37] Band engineering materials, had been proved to have remarkable figure of merits.[38,39] Composites and alloys, due to their relatively low thermal conductivities and high electric conductivities compared with their bulk counterparts, have attracted extensive interests.[40-47] Low dimensional nanostructures had been confirmed to exhibit good thermoelectric performance.[48-53] These materials provided a promising building block for practical thermoelectric applications in nanoelectronics.[12] Especially, reducing the scale of the material had a huge impact on its thermoelectric property, which could be explained as following:[14,33,54] i) improvement of the density of states near the Fermi level owing to the quantum effect, and thus the enhancement of Seebeck

RSC Advances Accepted Manuscript

coefficient compared to the bulk materials. ii) severe phonon scattering at the interfaces and boundaries, resulting in decreasing thermal conductivity.

From published papers, most of thermoelectric materials have ZT value of around 1.0.[55-57] For power generation, an optimistic energy conversion efficiency of the thermoelectric materials at heat source temperature about 750 K was predicted to be 30% when the ZT value reached 4.0, which would be an attractive choice for energy harvesting.[58] In experimental measurements, the ZT values of 1D nanostructures based on Bi-Sb-Te-Se complexes were in the range of 1.5-2.5.[59-61] Surface rough silicon (Si) NW exhibited a ZT of 0.6 at the room temperature while the ZT value of bulk Si was about 0.01.[25] The ZT value of single-crystalline β-SiC NWs was measured to be 0.12, which was around 120 times higher than the reported maximum value of bulk β-SiC.[62] From theoretical calculation, Bi_2Te_3 1D quantum wire with width 5 Å square cross section had a ZT up to 14.[15] Based on the quantum-limited effect of electrons and phonons, the ZT of bismuth NT with 10 nm diameter and 2 nm thickness was theoretically predicted up to about 6.[63] The ZT of $Si_{1-x}Ge_x$ NWs, oriented along the [110] direction with rectangular cross section area of 2.3 nm^2, was theoretically predicted to be above 4.[64] Furthermore, the room temperature ZT of a 1.1 nm diameter GaAs NW was predicted to reach as high as 1.34, exhibiting more than 100-fold improvement over the bulk counterpart.[65] The ZT of ZnO NW increased 30 times compared with its bulk, when its diameter decreased to 8 Å.[66] Therefore, it was a possible approach to improve thermoelectric performance by converting bulk material into 1D nanostructures.

I-3 Methods for measuring thermoelectric properties

Although great progress has been obtained in increasing thermoelectric figure of merit of 1D nanostructural material,[37,67,68] thermoelectric propriety measurements of nanoscale materials and devices were still a severe challenge. This might be attribute to the difficulty in dealing with the fabrication of measuring structures, issues of electrical contacts and the signal noises from nanostructural devices. Therefore, the measuring methods must be improved and optimized so as to explore high performance thermoelectric materials. Along with the technological development, the properties of thermoelectric materials with scale decreasing to a few microns or even a few nanometers, could be characterized. Hitherto, several methods have been developed to measure the thermal properties of NWs, such as self-heating 3ω method,[69] thermal flash method,[70] and the method using a suspend micro-device[71-73] In additional, a few reviews had been reported involving thermoelectric properties and structures of NWs.[74-80] Only few reviews, however, involved the measuring methods of thermoelectric properties of 1D nanostructural materials.[81-83]

This review explored the latest research results on the measuring methods for thermoelectric properties of 1D nanostructural materials. Five often used methods to measure Seebeck coefficient would be discussed. Similarly, twelve kinds of the most popular methods to measure thermal conductivity would be described. In each method, its principle, applications, merits and shortages would be presented in order to provide a comprehensive understanding of the method. Furthermore, two potential hot topics in measuring the 1D nanostructure thermoelectric properties would be proposed.

II Measurements of Seebeck coefficient of 1D nanostructural material

RSC Advances Accepted Manuscript

An accurate measurement of the Seebeck coefficient was essential with the aim to investigate and evaluate thermoelectric properties of new materials. However, measuring the Seebeck coefficient of an individual NW was fraught with difficulty for the requirement to extract the Seebeck voltage, ΔV, and temperature drop, ΔT, across the NW precisely. Therefore, there were at least two challenges associated with the measurement of Seebeck coefficient. One was applying a sufficient temperature difference along the NW, and another was measuring the Seebeck voltage accurately, which was a few microvolts.

In this section, five methods for measuring the Seebeck coefficient of NWs would be discussed. The methods using mesoscopic or microfabriccated suspended device had been extensively used and various similar devices had been built during the last decade. Methods using thermocouples or reference films were developed to characterize the Seebeck coefficient of NWs, offering other accesses to obtain the temperature difference besides temperature coefficient of resistance (TCR =(dR/dT)/R). The last method using ac signal could suppress unwanted noise so to improve the measuring accuracy. The discussions below focused on the principles of these methods. Furthermore, the main advantages and disadvantages of the methods were presented as well as their applications. A summary of these methods was presented in Table 1.

Table 1 Summary of measurements of Seebeck coefficient of 1D nanostructural material

Methods	Source	Sensor	Merits	Shortages	Ref
Mesoscopic device	Direct current (DC)	Based on TCR	Simple device Easy sample placement	Long thermal stabilization period Extra effort to achieve ohmic contact	[16] [21]
Microfabriccated suspended device	DC	Based on TCR	Thermal stabilization within several seconds	Complex device Difficult sample placement Extra effort to achieve electrical contact	[73] [110]
Mircodevice with thermocouples	DC	Thermocouple	The temperature obtained near the contacts	Careful noise cancelling and circuit design for thermocouple	[114] [115]
Measurement with a reference film	DC	Based on a reference film	Without direct temperature measurement	Difficult to achieve electrical contactExtra effort to obtain the S_R and S_C	[117] [118]
2ω technique	Alternating current(AC)	Based on TCR	Simple device High signal/noise ratio	Small singal at high frequency	[111] [119]

RSC Advances Accepted Manuscript

II-1 Mesoscopic device

II-1.1 Structure

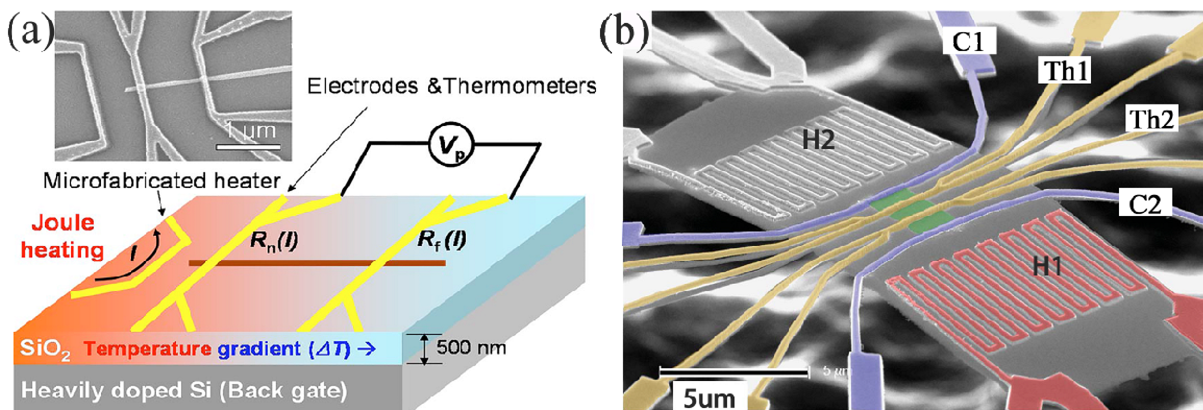

Fig. 1 Mesoscopic devices for measurement of Seebeck coefficient of individual 1D nanostructure: (a) Typical device with platinum(Pt) line heater; (b) Scanning electron micrographs of a device used to quantitate the thermopower of the NW. Reprinted with permission from ref. 84 and 16, AIP Publishing LLC and Nature Publishing Group.

In this method, a schematic layout of a typical structure for the Seebeck coefficient/TEP measurement, as well as its scanning electron microscope (SEM) image, was shown in Fig. 1(a). The NW was placed on a silicon oxide/silicon (SiO_2/Si) substrate and then followed by a deposition of two metallic wires (e.g. Pt) contacting both ends of the NW. These wires, in a four-probe configuration, were served as both electrodes and thermometers. To generate Joule heat, a microfabricated heater was fabricated adjacent to one of the NW-wires contacts. A direct current (DC), I, was applied to this heater and raised the temperature locally around the neighboring contact area. Furthermore, temperature gradient (ΔT) would be obtained from the resistances of the two thermometers, R_n and R_f, based on their TCR which had been previously calibrated. Fig. 1(b) showed another device which was almost the same as the former. However, two zigzag heaters, labeled as H1 and H2, were symmetrically fabricated. Four metallic wires (C1, C2, Th1 and Th2) comprised 4-point electrical contacts to characterize the electrical property of the NW. In additional, it was worth noting that Th1 and Th2 also served as resistive thermometers.

II-1.2 Principle

This Seebeck coefficient measurement relied on the heater to provide temperature difference across the NW. Once a direct current, I, crossed through the heater as schematically illustrated in Fig. 1(a), the temperature around the adjacent contact area would rise as a consequence of Joule heating. Part of the heat flowed through the NW and the SiO_2 layer, creating a temperature gradient along the NW. Then, instruments (voltage and current meters) were implemented to read resistances of the thermometers as well as the resultant thermoelectric voltage, ΔV (TEV), simultaneously.[85] Next, temperature gradient, ΔT, between the two thermometers was calculated based on the relationship between the thermometers' resistances and temperatures. The temperature of the thermometer was a function of the TCR, so, the resistance measured could be converted to average temperature of the thermometers direct.[21] Consequencely, the TEP could be obtained from equation (1-1).

RSC Advances Accepted Manuscript

Before carrying out the measurement, it was necessary to determine the relationship between resistance and temperature of the thermometer. In other words, the TCR needed to be determined.[86] For this purpose, four point probe technique was adopted.[73] Shin et al.,[85] for example, used four-probe to assure a significant improvement in accuracy. Compared with two-point-probe technique, the contact contribution and the resistance of wires outside the substrate could be eliminated when four point probe technique was used. Therefore, it was possible to obtain accurate signals through the resistances of the thermometers.

II-1.3 Merits and shortages

In order to minimize the heat loss due to air convection, the device was put in a vacuum chamber. Furthermore, the temperature difference along the NW provided by the heater was sufficient to facilitate the Seebeck coefficient measurement. Therefore, a tight control of energy flow in the device was not necessary.[87] Another merit was that the NW was put on the substrate followed by the deposition of metallic wires which resulted in easy sample placement. However, the Seebeck voltage, ΔV, was small (a few millivolts) and was measured by a nanovoltmeter. What's more, the major error source in this method would be ΔT due to various noises, for instance, the fluctuation of ambient temperature and the rectification of TCR. Therefore, low noise configuration was required for an accurate measurement of the Seebeck coefficient, for example, high vacuum and lock-in amplifiers for measuring the resistance of the temperature sensors. It was worth noting that this method required a thermal stabilization period after a heating power change, and cannot avoid uncertainty when reading the temperature owing to the existence of the substrate.[85] To tackle this, Shin et al, removed the backside Si underlying the SiO2 layer, and the membrane structure allowed for faster thermal stabilization within several seconds relative to the traditional bulk substrate.[85]

Another difficulty was the formation of ohmic contacts which was historically a challenge for NWs. On the one hand, the contact at the interface of the electrode and NW was mostly nonideal because of the extremely small contact area ($< 0.05\ \mu m^2$) and the unsubstantial contact. On the other hand, the oxide layer existed on the surface of the NWs and Schottky barrier at the contact area increased the experimental difficulty.[84] It had been reported that a 40nn Bi NW would consist of a 25 nm crystalline Bi core and a 7 nm thick amorphous oxide coating which resulted in nearly $1\times10^6\ \Omega$ electrical contact resistance between the Bi NW and metal electrode.[88] Nevertheless, in order to accurately obtain the Seebeck coefficient, it was necessary to couple the NW and electrode with ohmic contact. From published papers, there were several methods to obtain ohmic contact. In most of the measurements, electrical contacts were formed by depositing noble metals, such as Pt and tungsten (W), or carbon (C) films using focused ion beam (FIB) or Electron Beam Induced Deposition (EBID) due to its high accuracy on the selected region, followed by thermal annealing.[89] SEM and electrical measurements could be used to ensure the good ohmic contacts. For example, Valentin et al, utilized FIB to deposit Pt electrodes on the β-silicon carbide NW to obtain electrical contact.[90] Their SEM image showed that part of the NW was exactly covered by the deposited Pt and confirmed that an unsubstantial contact had been formed. It was noteworthy that FIB could also be used to expose the surface of the NW. Murata et al,[91,92] implemented a FIB processing to remove a selected portion of the quartz covered on bismuth (Bi) NW, and then deposit carbon films on the NW to form electrical contacts. The total contact resistances, however, based on their two-wire and four-wire measuring results, could be more than $2\times10^5\Omega$. Notablely, this approach was time consuming and might contaminate or even damage the NWs.[88,93] An

RSC Advances Accepted Manuscript

electrothermal annealing process prior to the measurement could also lead to the electrical contacts. Shapira et al.[94] used a staircase sweep of potential with steps of 0.5 V crossing the contact of a 30 nm nickel (Ni) NW and gold (Au) electrode to break down the native oxide until the resistance of the NW was dropped from its initial value of ~10^8 Ω to <10^4 Ω, which implied that the dielectrical contact resistance between Ni NW and Au could be approximately 10^8 Ω. The same process was also found in literature [95]. A DC voltage pulse of 1.5V for 0.5 s had been applied across the SiGe NW and aluminium (Al) contact. It was found that part of the NW became welded to the Al lead and was inserted into the metal due to Joule heating. Nevertheless, special attention should be paid to the voltage magnitude when a DC voltage was applied because the NWs was fragile and could be broken due to Joule heat. Additionally, it had been proved that thermal annealing and doping had a significant effect on metal-NW contact. For example, Yu et al.[96] found that, after thermal annealing, the measured resistivity could drop from 10^3 Ω cm to ~1Ω cm for Si NWs with Au contact. The thermal annealing process not only led to improved metal-NW contact but also facilitated NW doping via diffusion and ionization of the metal.[96] To obtain good ohmic contacts, other techniques had also been developed. Jang et al.[97] carried out an etching and depositing process of the electrodes without breaking the vacuum so as to prevent the further formation of the oxide layer. A proper plasma treatment was also used on the contact area prior to form electrical contact by Chul-Ho et al..[84] Interestingly, Wang et al.[98] developed a novel method to locally evaporate Pt metal between the NW and the electrodes using a shadow mask process.

II-1.4 Applications

The mesoscopic device was one of the most convenient and useful method to measure the TEP of a single NW, which could achieve both the temperature difference and measuring the Seebeck voltage. Small et al.,[21] in 2004, obtained the Seebeck coefficient of single wall CNTs (SWCNTs) using the microdevice and the measured thermoelectric power was ~ 200 μV/K at room temperature. Boukai et al.[16] fabricated a thermoelectric device platform to quantitate the thermopower and electrical conductivity of Si NW arrays, as shown in Fig. 1(b). The SiNW array was at the central area and under the wires (Th1 and Th2). The heaters were labeled as H1 and H2. Th1 and Th2 were 4-point devices which served as resistive thermometers. C1, C2, Th1 and Th2 comprised the 4-point electrical contacts to the Si NWs, with C1 and C2 utilized as the current source and drain for those electrical conductivity measurements. With this device, the TEP of Si NWs for cross-sectional area of 20nm×20nm was measured to be about 400 μV/K. More importantly, they found that ZT values representing an approximately 100-fold improvement over bulk Si are achieved including ZT ≈1 at 200 K. Lee, et al.[84] investigated the temperature-dependent TEP of individual wide band gap ZnO. The device the used was illustrated in Fig. 1(a). Their result showed that the TEP value of the ZnO NWs was as high as -400 μV/K at room temperature. Recently, Xu et al.,[99] utilizing this method, obtained the Seebeck coefficient of individual singlecrystalline SnTe NWs with different diameters ranging from ~218 to ~913 nm. The result showed that, when the diameter was decreased to 218 nm, the Seebeck coefficient turned out to be -41μV/K.

Compared with the line heater, platinum resistance thermometer (PRT) coil was designed to generate bigger temperature difference between both ends of the NWs (see Fig. 1(b)).[16,99,100] This makes the measurement of TEV easier. To obtain the temperature more accurately, two PRTs was adopted to alternately serve as the heat source.[72] In additional, scanning thermal microscopy (SThM) or numerical simulations are also used to correct the

RSC Advances Accepted Manuscript

measured temperature difference.[81,94,101] Furthermore, taking into account the temperature distribution over the structure, infrared image was used to directly obtain the temperature distribution of the device and this method was found to be appropriable to examine thermoelectric characteristics.[102]

Up to now, the mesoscopic structures had been successfully applied to characterize the thermoelectric properties of various NWs, such as Sb_2Te_3,[103] InAs,[100,104] GeSn,[105] InSb,[106] Ni [107] as well as fibres.[108]

II-2 Microfabricated suspended device

II-2.1 Structure

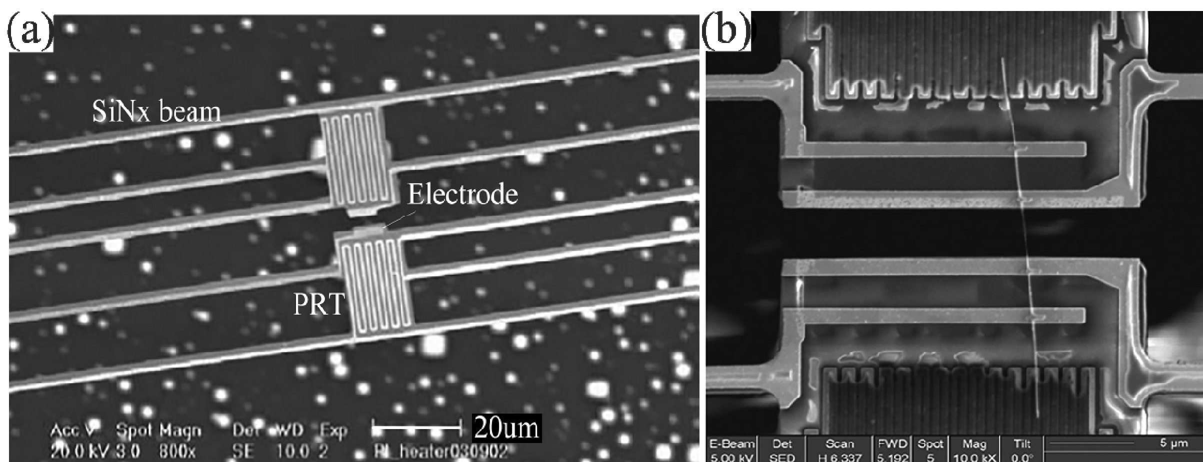

Fig. 2 (a) Microfabriccated suspended device and (b) SEM image of a SiC NW over the suspended microresistance thermometry device, platinum contacts are deposited on the NW-electrode contact area using ion beam induced deposition. Reprinted with permission from ref. 133 and 90, American Chemical Society and AIP Publishing LLC.

The outline of the suspended microstrcture device incorporated two adjacent thick ultra-low-stress Si nitride (SiN_x) platforms, each around 15 μm^2, suspended by several long (200-400 μm) and narrow (2-4 μm) SiN_x beams, as shown in Fig. 2(a). On each platform, a PRT was deposited and acted as not only a heater to achieve temperature difference but also as a thermometer. Furthermore, two electrodes were lithographically patterned for connecting the NW. Once a NW was placed on the device and bridged on the two electrodes designed on each island, the NW was connected to the outside pads via Pt wires deposited on each SiN_x beam. A SiO_2 film was deposited on top of the thermometers to isolate the NW from PRTs.[73,95] Fig.2(b) showed another device with a SiC NW suspending over the electrodes, platinum contacts are deposited on the NW-electrode contact area using FIB.[90]

II-2.2 Principle

In this suspended device, when a direct current flowed through one of the PRTs, the temperature at one end of the NW was increased by Joule heating. Part of the heat would flow through the NW and created a temperature gradient along the NW. The Seebeck voltage, ΔV, was, then, induced by the temperature gradient and could be

RSC Advances Accepted Manuscript

measured through the contact pads which connected the NW. Furthermore, the temperature difference ΔT could be obtained through the PRT's TCR. The Seebeck coefficient, consequently, determined from equation (1-1).

II-2.3 Merits and shortages

The microfabricated suspended device was a powerful tool for the measurement of one-dimensional nanostructures, offering significant advantages such as measuring Seebeck coefficient, electric conductivity and thermal conductivity of the same NW. One of the main outcomes of this device was that it provided an effective approach to measure the thermal properties of NWs with small diameter down to a few nanometres, for example, 10nm in ref. 73. Compared with the mesoscopic device, this suspended device allowed for faster thermal stabilization within several seconds after each temperature change due to thermal decoupling of the electrical heaters/sensors from the carrier substrate. However, this method involved additional preparation efforts such as the fabrication of these suspended devices and difficult sample placement. Complex processes and very specific equipments were required to fabricate the suspended structures. For example, more than five process steps and electron beam lithography were involved. Additionally, the devices in this method also ran into inevitable issues with controlled placement of the single NWs exactly between the two Pt electrodes designed on each island due to the small size of the NWs (<100 nm) and the suspended structure. From published papers, there were two main strategies to place the NWs. In the first strategy, the NWs were first dispersed into a volatile solvent by sonivation, and then dropped cast onto a wafer containing many suspended devices. After drying the solvent, statistically, some of the NWs were exactly adsorbed on the two Pt electrodes.[73,110] It was worth noting that high density of the devices on a wafer significantly improved the yield of testable NWs since the drop dispense method of NW deposition was inherently a random process.[111] In the second strategy, individual NWs were picked up by a tip from the hosting bundle, and then a nanomanipulator was used to place the NW at a desired location for characterization. Being highly selective and reproducible, this strategy, provided a reliable way to manipulate a single NW for certain applications.[62,112] Nevertheless, it was a time consuming work and special instruments were required, such as FIB and the nanomanipulator. Another difficulty was the formation of ohmic contacts. To reduce the electrical contact resistance between the NW and the electrodes, the FIB, thermal annealing and other novel strategies were adopted, which have been discussed in section II-1.3.

II-2.4 Applications

By employing this method, the Seebeck coefficient of individual SWCN bundle as a function of temperature were measured. it showed linear temperature dependence in the temperature range of 30–250 K, and saturated above 250 K.[73] To investigate the thermoelectric properties of Bi_2Te_3 NWs, Li et al.,[110] using this suspended microdevice, found the Seebeck coefficient of the 391 nm Bi_2Te_3 NW to be ~50 μV/K at room temperature, and the results showed it had the same trend as bulk Bi_2Te_3 material. Valentín et al.,[90] recently, investigated the thermal properties of β-SiC NWs as shown in Fig. 2(b). The temperature dependence of the Seebeck coefficient was studied, and the largest value for NW in 90 nm turned to be -68 μV/K at 370 K. Moreover, Lee et al.[113] simultaneously measured all thermoelectric properties of the SiGe NWs which exhibited a large thermoelectric ZT of ~0.46 at 450 K.

RSC Advances Accepted Manuscript

II-3 Mircodevice with thermocouples

II-3.1 Structure

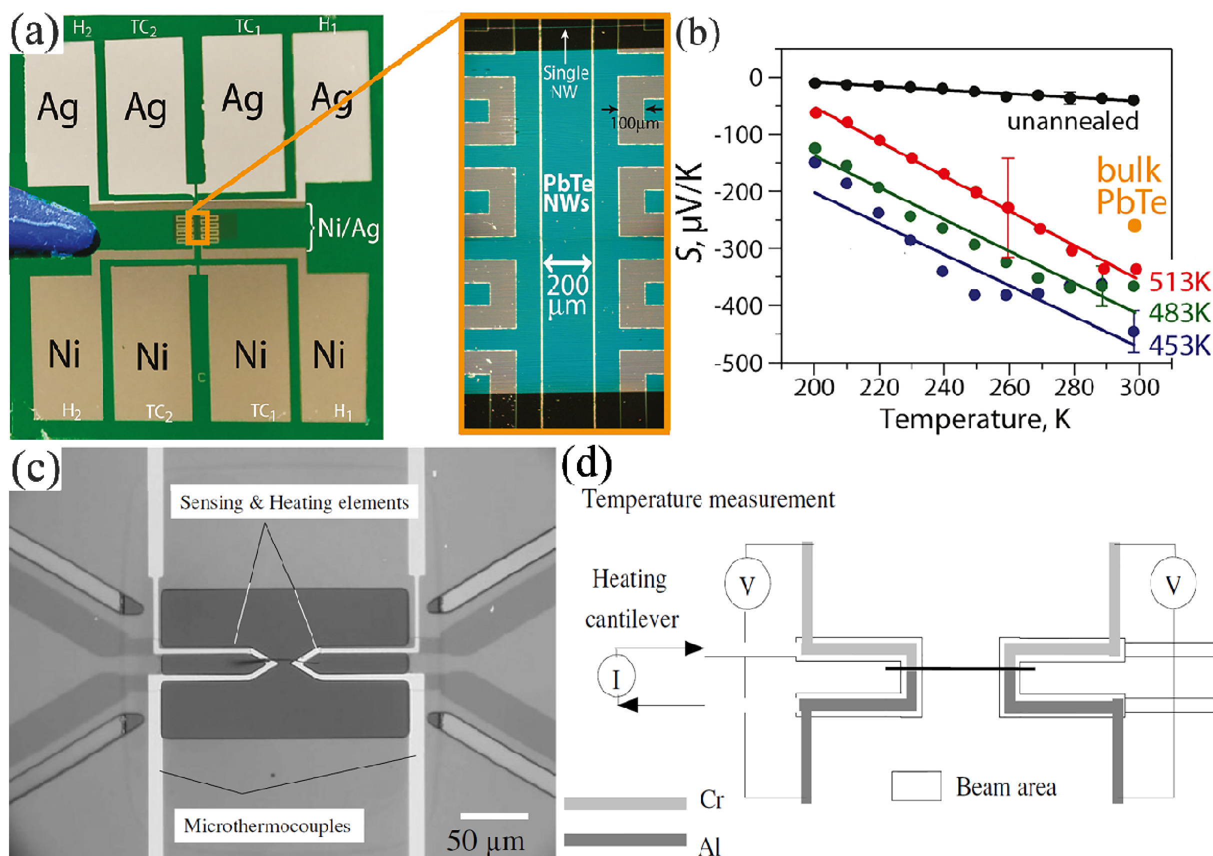

Fig. 3 (a) A device including two meander heaters and two Ag/Ni thermocouples for measurement of S and σ for NW arrays; (b) Plots of Seebeck coefficient against annealing temperature for PbTe NWs; (c) Photograph of the suspended microdevice for evaluating thermoelectric properties of nanomaterial; (d) Measurement of the temperature from the two microthermocouples in the short-circuit configuration during heating. Reprinted with permission from ref. 114 and 115, American Chemical Society and IOP Publishing.

A microfabricated device structures with thermocouples for the Seebeck measurement was shown in Fig. 3(a). The device consisted of two outside microfabricated heaters and two microthermocouples fabricated on a Si_3N_4 wafer. The NW was put under the two electrical contacts.

II-3.2 Principle

The individual NWs were placed between the two heaters for characterizing thermoelectric properties as shown in Fig. 3(a). In order to evaluate the Seebeck coefficient, the NWs were heated by feeding a current into the heater from either side. Therefore, a temperature gradient was then generated along the NWs. From the two electrical contacts, the Seebeck voltage and temperatures at two ends of the NW were measured individually. More specifically, the temperature difference, ΔT, of the NWs could be obtained from the two microthermocouples

RSC Advances Accepted Manuscript

(TC_1 and TC_2); the Seebeck voltage, ΔV, could be measured from the two electrical contacts. Finally, from the temperature difference ΔT and the Seebeck voltage ΔV, the Seebeck coefficient at a specific temperature could be approximated as[115]

$$S = \left| \frac{\Delta V}{\Delta T} \right| + S_{metal1} \qquad (2\text{-}1)$$

where S_{metal1} is the Seebeck coefficient of the metal contacted with the NWs.

II-3.3 Merits and shortages

It should be noted that the temperature difference of the NW could be obtained from the TCR of the heaters as described in sections above. However, it was difficult to make precise measurements of the temperature at the end of the NW since the temperature along the heater was nonuniform and the resistance was measured as an average value. As for the temperature sensor involved in this method, it conferred the advantage that the microthermocouple had the ability of precise temperature measurement at a very small area near electrical contact.[114] Additionally, thermocouple was ideal simple measurement device, with each temperature being characterized by a precise temperature-voltage curve, independent of any other details. Nonetheless, in reality, thermocouple was affected by issues such as ambient temperature fluctuation and circuit design mistakes. Furthermore, the NW had to be placed over/under the same metal, otherwise, the Seebeck voltage could not be accurately detected due to different contacts at two ends of the NW. It should also be pointed out that, before applying this measurement, the thermocouples should be calibrated.

II-3.4 Applications

Yang et al.,[114] using a device with two meander heaters and two thermocouples deposited on top of an array of ~200 PbTe NWs as shown in Fig. 3(a), analyzed the annealing effect of PbTe NWs. Fig. 3(b) showed that the measured Seebeck coefficient was -479 μV/K for annealed NWs which was 80% larger in magnitude than the Seebeck coefficient of bulk PbTe. Ono et al.[115] developed a platform with build-in microthermocouples to evaluate the thermoelectric properties of low-dimensional materials. As shown in Fig. 3(c), the device consisted of freely suspended heating elements opposite to each other, and a thermocouple integrated into the individual heating element. The temperature was obtained from two microthermocouples with a Cr–Al junction during heating, which was shown in Fig. 3(d). Their obtained Seebeck coefficient of a Bi_2Te_3 bundle was about 19 μV/K.

II-4 Measurement with a reference film

II-4.1 Structure

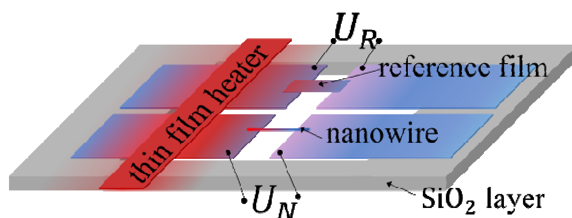

RSC Advances Accepted Manuscript

Fig. 4 Schematic diagram of Seebeck coefficient measuring device with a reference film.

The microchip was shown in Fig. 4, which consisted of two identical pairs of metallic contacts anchored on SiO_2 layer. A NW was suspended over one pair of them, and a reference film with a known Seebeck coefficient between the other. To generate a temperature between the NW and the film, a thin film heater was also designed beside the sample.

II-4.2 Principle

As shown in Fig. 4, a direct current was fed through the thin film heater in order to generate an identical temperature difference, ΔT, on both pairs of the contact film. With the reference film, the temperature difference between two ends of the NW could be determined through the reference voltage U_R of the Seebeck reference film,

$$U_R = \left(S_R - S_C\right)\Delta T \qquad (2\text{-}2)$$

where S_R and S_C are the known Seebeck coefficient of the reference film and the contact pads, respectively. Therefore, when the Seebeck voltage U_N of the NW was measured, the NW's Seebeck coefficient S_N could be obtained according to[116]

$$S_N - S_C = U_N / \Delta T = U_N \left(S_R - S_C\right) / U_R \qquad (2\text{-}3)$$

II-4.3 Merits and shortages

The main advantage of this method was that it avoided determining the temperature difference between two NWs contacts comparing with the TCR method. Thus, the influence of nonuniform temperature distribution could be minimized, if the device was properly designed, such as symmetrical structure. However, more effort should be done to investigate the Seebeck coefficient of the reference film and the contact pads at different temperature since they were required in this method. Furthermore, to obtain a correct Seebeck voltage, one had to solve the ohmic contact problem before applying this method. The Seebeck voltage could not be obtained if non-ohmic contacts were existed.[117] Depositing noble metals, such as Pt and Ti, using FIB, or annealing procedure were recommended to guarantee electrical contacts.[90,91]

II-4.4 Applications

Cronin et al.[117] used a reference film with known Seebeck coefficient to measure the Seeheck coefficient and resistivity of an individual Bi NW. The Seebeck voltage, however, could not be obtained owing to the high resistance of the non-ohmic contacts. Volklein et al.[118] further developed this method and carried out a simulation to demonstrate that temperature differences between two ends of the NW could be obtained. Furthermore, together with a steady-state dc thermal bridge method (DCTBM), this measurement was further developed to investigate the thermoelectric transport coefficient S, κ and σ of NWs, so to obtain the figure of merit ZT of the measuring material.[116]

II-5 2ω technique

RSC Advances Accepted Manuscript

II-5.1 Structure

The related schematic of the device structures for the Seebeck coefficient measurement in a vacuum was shown in Fig. 1(a). The device consisted of one microfabricated heater and two thermometers patterned on a Si substrate covered with a thin SiO_2 layer.

II-5.2 Principle

When an ac current at frequency ω was fed into the mircoheater, which resulted in Joule heating with a frequency 2ω. This heat diffusion caused a temperature oscillation which propagated through the substrate to the NW. Therefore, a temperature difference was established, and both the temperatures associated with the frequency 2ω. $T_H(2\omega)$ and $T_L(2\omega)$, at two ends of the NW could be determined by measuring four-probe resistance of the Pt wires. Consequently,the temperature difference $\Delta T(2\omega)$, could be obtained by

$$\Delta T\left(2\omega\right) = T_H\left(2\omega\right) - T_L\left(2\omega\right) \qquad (2\text{-}4)$$

Employing lock-in amplifiers, both the Seebeck voltage $\Delta V(2\omega)$ and $\Delta T(2\omega)$ could be measured. Finally,the Seebeck coefficient, S, of the NW calculated as[119]

$$S = -\frac{\Delta V(2\omega)}{\Delta T(2\omega)} \qquad (2\text{-}5)$$

II-5.3 Merits and shortages

The thermoelectric power measurement essentially incorporated reading the voltage generated by a temperature gradient. In order to produce the temperature gradient, the described method used the AC current to heat the heater via Joule heating. By employing a lock-in amplifier to obtain the 2nd harmonic voltage, the influence of environmental factors, such as temperature and pressure fluctuation, was minimized due to the high signal/noise ratio of the lock-in amplifier. Furthermore, the Seebeck voltage, $\Delta V(2\omega)$, was clearly proportional to the temperature difference, $\Delta T(2\omega)$, without any offset, because there was no phase lag between them.[119] Nevertheless, it should be noted that, as the frequency increased, the temperature fluctuation amplitude (although the average temperature over time would remain the same) would be decayed, resulting in a reduction of measured thermoelectric voltage.[111] As a result, the frequency in this method was recommended below the inverse of the thermal time constant of the heater. For example, below 1kHz in ref. 111. Additionally, if a bulk substrate device was adopted, a period of time to build thermal equilibrium was required. This situation could be improved by the suspended structure.

II-5.4 Applications

Duarte et al.[111] measured the Seebeck coefficient of an individual NW with this method. In their measurement, the mircoheater and the NW were suspended to prevent substrate-coupling effects.[73,120] In additional, they also observed thermopower enhancement in"junctioned" gold NWs near room temperature.[23] Kirihara et al.[119] recently fabricated a device with Pt microelectrodes and microheater. It was reported that the Seebeck coefficient of single-crystalline boron nanobelt (20 nm in average thickness) was measured to be 174 μV/K at 300k. Furthermore, the thermopower of quantum dots defined in heterostructure NWs were also measured so to obtain a comprehensive understanding of the quantum dot's thermopower as a function of the Fermi energy.[121,122]

RSC Advances Accepted Manuscript

III Measurement of thermal conductivity of 1D nanostructural material

In this section, twelve measurements of thermal conductivity of 1D nanostructural material were covered. The method with microfabriccated suspended device, 3ω method and transient electrothermal method (TET) had been extensively used and the thermal conductivities of various NWs had been measured by these methods.[69,73,123] T-type nanosensor method was initially developed to characterize the thermal conductivity of a carbon nanotube and was later developed to measure the thermal conductivity of a NW. the DCTBM could be utilized to evaluate both conductive and nonconductive fibers. When compared with the existing techniques, this method appeared to present a reasonable alternative due to its simplicity and a high degree of reliability.[124] Optical heating and electrical thermal sensing method (OHETS) was developed to characterize the thermal diffusivity of individual nonconductive submicron/nanoscale wires/tubes. Transient photoelectrothermal (TPET) and pulse laser-assisted thermal relaxation (PLTR) techniques were both based on laser irradiation and featured significant signal/noise ratio in millivolts.[125] Measurements based on Raman thermography or thermoreflectance techniques were methods that could be used to measure absolute temperature. With these noncontact temperature measuring methods, the influence of thermal contact resistances could be eliminated. Thermal flash method could be carried out without calling for any knowledge or estimate of the interfacial/contact resistances.[126] 3ω-scanning thermal microscopy (SThM) technique which was based on third harmonic voltage at the thermoresistive probe could obtain the thermal conductivities of a wide range of individual NWs embedded in a matrix.

This section briefly introduced the principles of these methods. The main advantages and disadvantages of the methods were presented as well as their applications. A summary of these methods was presented in Table 2

RSC Advances Accepted Manuscript

Table 2 summary of measurements of thermal conductivity of 1D nanostructural material

Methods	Principle	Samples in references	Uncertainty	Merits	Shortages	Ref
Microfabricated suspended device	MEMS Steady-state method	Conductive NWs Minimum diameter 10 nm [73] Thermal conductivity from 1.1 to 3000 W/mK [128,129]	>9% [73]	Platform for the Seebeck coefficient, electrical and thermal conductivity Measurement sensitivity down to ~1pW/K with special configuration[112,140]	Complicated structure Difficult sample placement Extra effort to achieve ohmic contact Influence of the unknown thermal contact resistance	[71] [73] [140]
3ω method	3ω theory Dynamic method	Conductive NWs Minimum diameter 45 nm [189] Thermal conductivity from 0.5 to 830 W/mK [159,189]	9% [191]	Simple structure Convenient manufacture High signal-to-noise ratio	Exist truncating error and radial heat loss Difficult for nonconductive NWs Low signal level (μV)	[69] [191]
T-type nanosensor	1D transient conduction theory Steady state method	Conductive NWs Minimum diameter 9.8 nm [195] Thermal conductivity from 110 to 2000 W/mK [199,195]	7% [196]	Simple structure Thermal contact resistance could be theoretically extracted	Insufficient sensitivity with small diameters Considerable influence of the thermal contact resistance	[195] [199]
DCTBM	1D transient conduction theory Steady state method	Conductive fibers Nonconductive fibers (additional metallic coating) Minimum diameter ~15 μm [205] Thermal conductivity from 7	11% [124]	Simple structure High degree of reliability Both conductive and nonconductive fibers	Only larger fibers had been measured Difficult to evaluate the thermal contact resistance	[124]

RSC Advances Accepted Manuscript

		to 27 W/mK [205,124]				
OHETS	1D transient conduction theory Dynamic method	Conductive fibers Nonconductive fibers (additional metallic coating) Minimum diameter ~800 nm [207] Thermal diffusivity from 1.05×10^{-7} to 6.54×10^{-5} m^2s^{-1} [207,206]	10% [206]	Simple structure Both conductive and nonconductive sample Neglectful effect of the laser beam distribution	The thermal diffusivity was obtained rather than the thermal conductivity Low signal level (μV) Complex configurations	[206] [207]
TET	1D transient conduction theory Transient method	Conductive fibers Nonconductive fibers (additional metallic coating) Minimum diameter ~324 nm [211] Thermal diffusivity from 1.53×10^{-7} to 6.67×10^{-5} m^2s^{-1} [211,123]	10% [123]	Simple structure Both conductive and nonconductive samples Strong signal level	Only for the thermal diffusivity Nonconstant heating power due to the variation of sample resistance The results depended on the the rising time of the electric current	[123] [215]
TPET	1D transient conduction theory Transient method	Conductive fibers Nonconductive fibers (additional metallic coating) Minimum diameter 10.4 μm [218] Thermal diffusivity from 5×10^{-7} to 2.53×10^{-5} m^2s^{-1}	-----	Simple structure Both conductive and nonconductive samples Strong signal level	Only for the thermal diffusivity Only larger fibers had been measured The results depended on the the rising time of the laser beam	[218]

RSC Advances Accepted Manuscript

		[218]				
PLTR	1D transient conduction theory Transient method	Conductive fibers Nonconductive fibers (additional metallic coating) Minimum diameter 23 μm [210] Thermal diffusivity 1.05×10^{-5} m^2s^{-1} [210]	10% [209]	Simple structure Both conductive and nonconductive samples Negligible influence of the laser beam's rising time	Only for the thermal diffusivity Only larger fibers had been measured	[209] [210]
Raman Thermography	Raman Thermography Steady state method	Conductive NWs Minimum diameter 1.8 nm [220] Thermal conductivity from 0.44 to 2630 W/mK [227,127]	14.41% [227]	Simple structure Negligible influence of the thermal contact resistance	Limited resolution of the Raman spectrometer Raman spectrum should be corrected before measurements	[127] [220]
Thermal flash method	Thermal flash Transient method	Conductive fibers Nonconductive fibers Minimum diameter presented in this work 271nm [70] Thermal diffusivity from 5.97×10^{-8} to 1.78×10^{-3} m^2s^{-1} [70,126]	-----	Both conductive and nonconductive samples Without concern for thermal contact resistance	The thermal diffusivity was obtained rather than the thermal conductivity Limited by the data acquisition rate	[70] [126]
Thermoreflectance Technique	Thermoreflectance Technique Steady state method	Conductive NWs Minimum diameter presented in this work 115 nm [238]	-----	0.1 °C temperature resolution Without concern for thermal contact resistance	Limited by the spatial resolution of the thermoreflectance	[238]

RSC Advances Accepted Manuscript

		Thermal conductivity 46 W/mK [238]			Thermoreflectance coefficient should be calibrated	
SThM Technique	3ω-SThM Dynamic method	Conductive NWs Minimum diameter presented in this work 120nm [247] Thermal conductivity from 0.5 to 128W/mK [247,241]	-----	Spatial resolution around 100 nm Non destructive method	Consequential effect of the thermal contact resistance Complex theoretical models	[241] [244]

RSC Advances Accepted Manuscript

III-1 microfabricated suspended device

III-1.1 Structure

The outline of the suspended structure was shown in Fig. 2(a) which has been described in section II-2.1. In this method, the suspended structure was loaded into a cryostat with an ambient pressure less than 1×10^{-5} Torr to ensure that the heat loss from the NW to ambient environment by convection was negligible.

III-1.2 Principle

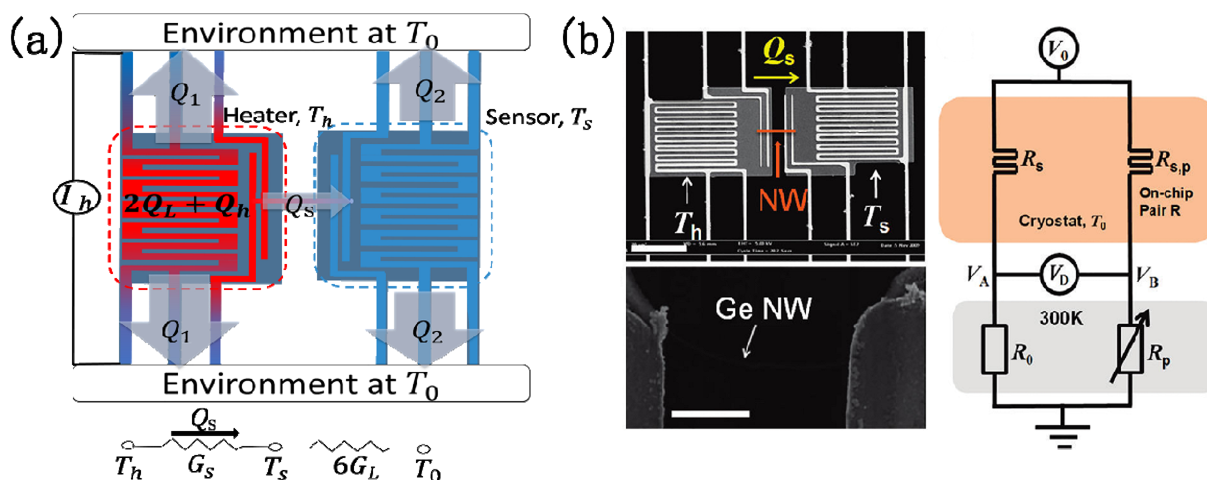

Fig. 5 (a) Schematic of energy exchange, for the heater at T_h, and the sensor at T_s; (b) Experimental setup of the Wheatstone bridge circuit for NW thermal measurement. Reprinted with permission from ref. 128, American Chemical Society.

In this typical method, a dc current, I_h, was applied to the suspended heater so that the heater's average temperature, T_h, was elevated above the ambient temperature, T_0, as shown in Fig. 5(a). With the PRT's TCR, the temperature, T_h, of the heater could be obtained by measuring the resistance of the heater, R_h, through the standard four-probe method. At the same time, the temperature of the sensor, T_s, was determined using a lock-in amplifier which generated a very small probing current so that the Joule heat of the sensor could be ignored.

To determine the thermal conductivity of the NW, some assumptions were put forward as following:[73]

i) The temperature of the heater or sensor was uniform.

ii) The heat transfers between the two membranes by air conduction, convection and radiation were negligible.

iii) The temperature at the junction between each beam and the substrate was equal to the substrate temperature which was considered to be a constant,T_0,

With the assumptions above, the energy exchange could be given as Fig. 5(a), where Q_h and $2Q_L$ are the Joule heat of heater and two Pt wires generated by the current, I_h, respectively. Simultaneously, the Joule heat rose the temperature of the heater by ΔT_h ($\equiv T_h$-T_0). Then, a certain part of heat (Q_s) was conducted through the NW from the heater to the sensor which rised the temperature of sensor by ΔT_s($\equiv T_s$-T_0), and it was further transferred to the ambiance through the six beams supporting the sensor ($2Q_2$). Furthermore, it was noteworthy that Q_s was equal to

RSC Advances Accepted Manuscript

$2Q_2$. Another part of the heat, $2Q_1$, was conducted away through the six beams which connected to the heater. Hence, the energy conservation was invoked as

$$2Q_1 + 2Q_2 = Q_h + 2Q_L \quad (3\text{-}1)$$

With careful calculation, one could find that the thermal conduction of beams which suspended the sensor, G_b, could be obtained as

$$G_b = \frac{Q_h + Q_L}{\Delta T_h + \Delta T_s} \quad (3\text{-}2)$$

From the thermal resistance circuit shown in Fig. 5(a), thermal conduction of NW, G_s, could be determined as[73]

$$G_s = G_b \frac{\Delta T_s}{\Delta T_h - \Delta T_s} \quad (3\text{-}3)$$

Thus, the thermal conductivity of NW, κ_s, was obtained by

$$\kappa_s = \left(Q_h + Q_L\right) \cdot \frac{\Delta T_s}{\Delta T_h^2 - \Delta T_s^2} \cdot \frac{l}{A_s} \quad (3\text{-}4)$$

where l and A_s are the length, and cross section area of the NW sample, respectively. Additionally, temperature changes in each membrane (ΔT_h and ΔT_s) could be obtained from the measured resistances of the heater and sensor. Q_h and Q_L could be calculated from the direct current passing through the heater and the measured resistance of the heating PRT as well as the Pt wires on the beams.

III-1.3 Merits and shortages

One of the main merits of these suspended devices was that they could access not only to the thermal conductivity but also to the Seebeck coefficient and the electric conductivity of the same individual NW. Hence, these nanostructures offered a convenient route to obtain the figure of merits of the NWs. Furthermore, the influence of the substrate could be minimized by suspended geometry. Heat transfer between the two membranes via radiation and air conduction were well below the measurement sensitivity (~1nW/K) at 300k and were negligible when the suspended structure was enclosed in a cryostat with a vacuum level better than 1×10^{-5} Torr.[73]

Ever since this method was introduced,[129] various approaches had been developed to improve the accuracy of the measurement, such as estimate of the thermal contact resistances,[130-132] and using a Wheatstone bridge to cancel the temperature fluctuation.[128] The measurement sensitivity of the standard devices had been demonstrated to be ~1nW/K.[73] However, Consider the case of a NW with very small diameter (e.g. 10nm) and thermal conductivity as low as 1 W/mK, the thermal conductance would be 10 times lower than the sensitivity. Consequently, this method was feasible only when the thermal conductances of the NWs were larger than the sensitivity of the device. For instance, NTs[133] and NWs with the thermal conductances lager than 1nW/K.[134,135] This limitation may be attributed to several reasons, including temperature noise of the device, parasitic heat loss, etc.[82,136] Therefore, highly sensitive, micro-fabricated suspended devices were required to obtain thermal conductivities of single NWs with smaller diameter NWs, which may exhibit ultra-high figure of merit due to the quantum size effects.[137-139] To this end, noise-canceling schemes had been exploited to cancel the temperature fluctuation in the sample environment, and, consequently, significantly enhanced this thermal bridge method capable of measuring thermal conductance values down to ~1pW/K.[140,141] Very recently, careful calculation and

RSC Advances Accepted Manuscript

measurement had been also carried out to measure the NW samples with a low thermal conductance in the order of 10^{-10}W/K.[71,112]

The presence of an unknown thermal contact resistance between the NW and the contact electrodes was also a critical issue. There have been a few reports on molecular dynamic (MD) simulations and experimental investigations of the thermal contact resistance of the NW and CNT. For example, the thermal contact resistances of ZnTe NW with a diameter of 145.6 nm were obtained through the MD simulation, which were around 20% and 5% of the total measured thermal resistance before and after Pt contact deposition, respectively.[142] While another simulation implied that the thermal contact resistance of ZnTe NW with the same diameter was about 10% of the total measured thermal resistance and reduced to 3% after the Pt contact deposition.[143] The different results might attribute to discrete simulation parameters. Shi et al.[73] estimated the contribution of thermal contacts with Pt deposition to be less than 15% for 100nm SiNW. Additionally, for a 66 nm diameter multiwalled carbon nanotube, experimental result showed that thermal contact resistance could contribute up to 50% of the total measured thermal contact resistance.[130] In practice, the thermal contact resistance could be much larger than the value of simulation or estimated due to nonideal contact.[144] There were two main reasons that made this thermal contact resistance a challenge for measuring the thermoelectric properties of the NWs. First, when the contact area between the NW and the contact material became comparable to the mean free path of phonons or electrons, the thermal contact resistance would consist of an additional ballistic or interface resistance component besides the diffusive component given by the Fourier's law.[144] Second, the contact at the interface was nonideal for the extremely small contact area ($< 0.05\ \mu m^2$). A conventional method to decrease the thermal contact resistance was depositing metallic material, such as Pt and W, on top of the contact using FIB so that the NW was sandwiched between two metallic layers since metals were good conductors of heat through electrons.[145] Furthermore, careful examination of the contact condition was recommended so as to ensure that the obtained thermal conductivity did not deviate from the intrinsic thermal conductivity of the NW significantly.

III-1.4 Applications

To date, this method had been utilized to determine a number of NWs with various characteristics,[146-151] and various materials. For example, CNTs,[109] SiGe,[113] Bi,[152,153] Bi_2Te_3,[154] PbTe,[155,156] InAs,[53,157] and ZnTe,[142,143] had been investigated using this suspended microdevice for the measurement of their thermal properties.

Kim et al.[129] measured the thermal conductivity of an individual MWNT of a diameter 14 nm using this microfabricated suspended device. The observed thermal conductivity was more than 3000W/K m at room temperature. The measurements were also performed with a 10 nm and a 148 nm SWCN bundles by Shi et al..[73] The observed thermal conductivities were low compared to that of an individual MWCN, and for the 148 nm bundle, the thermal conductivity exhibited a $T^{1.5}$ in the temperature range of 20–100 K. More recently, Wingert et al.,[128] using their suspended device with Wheatstone bridge circuit(See Fig. 5(b)), obtained the thermal conductivities of Ge and Ge−Si core−shell NWs with diameters less than 20 nm. The measured thermal conductivity for the 15 and 19 nm Ge NWs were (1.54 + 0.59/−0.30) and (2.26 + 0.60/−0.39) W/mK, respectively. And the thermal conductivities of the Ge−Si core-shell NWs were in the range of 1.1~2.6 W/mK at 108~388 K.

III-2 3ω method

RSC Advances Accepted Manuscript

III-2.1 Structure

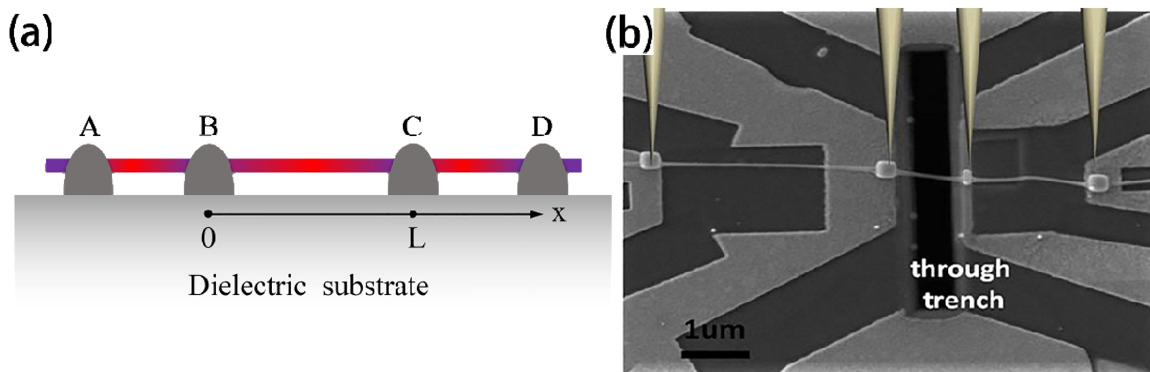

Fig. 6 (a) Illustration of the four-probe configuration for measuring the specific heat and thermal conductivity of NW; (b) a SEM picture showing the nanoscale four-point probe for the 3ω measurement. Reprinted with permission from ref. 62, Springer.

The NW sample was freely suspended across four electrodes in a four-probe configuration on a dielectric substrate. As shown in Fig. 6(a), the two outside electrodes, A and D, were used for feeding a sinusoidal electrical current, $I_0\sin(\omega t)$, and the two inside ones, B and C, were utilized for measuring the voltage across the sample.

III-2.2 Principle

The NW sample was freely suspended across four electrodes in a four-probe configuration and fed by a sinusoidal electrical current, $I_0\sin(\omega t)$, through the two outside electrodes, A and D, as shown in Fig. 6(a). As long as the current passed through the NW, the temperature fluctuation would be at frequency 2ω due to that the Joule heat was proportional to $[I_0\sin(\omega t)]^2$. Taking into account the NW's TCR, the evoked harmonic resistance of the sample would fluctuate at frequency 2ω as well. Therefore, a small 3ω voltage signal between the two inside electrodes (B and C), $V_{3\omega,RMS}$, could be detected by a lock-in amplifier, from which the specific heat and thermal conductivity could be determined. In additional, the sample was put in a vacuum chamber to prevent heat loss from the NW to ambient environment by air convection.

No external heater was required since most of the thermoelectric NWs were semiconductors, and themselves could sever as not only heaters but also sensors. However, the samples needed to be suspended in a high vacuum so as to allow the temperature fluctuation and avoid heat loss into the environment. Also, the electrodes had to be highly thermal conductive, so to heat sink the energy at these four points to substrate.[69] In such case, the temperatures at the four electrodes were assumed to be stable at ambient temperature, T_0. The heat was considered to diffuse along the NW and the one-dimensional transient conduction equation along the sample suspended between two inside electrodes was written as[69]

$$\begin{aligned}\rho C_p \frac{\partial}{\partial x^2} T(x,t) - \kappa \frac{\partial^2}{\partial x^2} T(x,t) \\ = \frac{I_0^2 \sin^2 \omega t}{L A_s}\left[R_0 + R'\left(T(x,t) - T_0\right)\right]\end{aligned} \quad (3\text{-}5)$$

RSC Advances Accepted Manuscript

where ρ, C_p, κ and R_0 are mass density, specific heat, thermal conductivity and electric resistance of the NW, respectively. $R'[=(dR/dT)_{T_0}]$ is the temperature gradient of the resistance at ambient temperature, T_0, L is the length of the NW between the two inside contacts, t means time, and A_s is the cross section of the NW.

From equation (3-5), the 3ω signal generated in the NW, $V_{3\omega}=IR=I(R_0+\delta R)$, was expressed as

$$V_{3\omega,RMS}=\frac{4I_{\mathrm{RMS}}{}^{3}LR_0R'}{\pi^4\kappa A_S\sqrt{1+(2\omega\gamma)^2}} \quad (3\text{-}6)$$

where γ is a constant. When the measurement was performed at low frequency limit $\omega\gamma\rightarrow 0$, $V_{3\omega}$ was nearly frequency independent. Therefore, (3-6) could be expressed as a simpler expression,[69]

$$V_{3\omega,RMS}\cong\frac{4I_{\mathrm{RMS}}{}^{3}LR_0R'}{\pi^4\kappa A_S} \quad (3\text{-}7)$$

Consequently,

$$\kappa=\frac{4I_{\mathrm{RMS}}{}^{3}LR_0R'}{\pi^4V_{3\omega,RMS}A_S} \quad (3\text{-}8)$$

According to (3-6), as the frequency decreased, the magnitude of $V_{3\omega,\mathrm{RMS}}$ would gradually increase and eventually reached a frequency-independent value. This had been verified in a number of experiments.[158,159] For this reason, one could obtain the thermal conductivity κ of a NW by fitting the experimental $V_{3\omega}$ data to equation (3-6) with the measured frequency. Another strategy, by taking advantage of the relationship, $V_{3\omega,\mathrm{RMS}} \sim I_{\mathrm{RMS}}{}^3$, to obtain κ was measuring the $V_{3\omega,\mathrm{RMS}}$ values with different ac electrical currents at a low angular modulation frequency.[160-162]

III-2.3 Merits and shortages

The 3ω method had become a common method to determine the thermal physical properties because of its relatively simple structure and convenient manufacture. Furthermore, it had better signal-to-noise ratio (SNR) compared with the suspended device by employing a narrow-band detection technology, which had an advantage of eliminating spurious signals. The thermal contact resistance was negligible in this method, because they could only shift the amplitude of the signal, but not the frequency. However, analytical expression deducted by Lu et al.[69] would introduce errors due to oversimplification and approximation, for instance, truncating part of terms of the infinite series and, furthermore, neglecting the radial heat loss. Special care was required when using this approach considering the truncating error and radial heat loss. Therefore, several improved models for measuring the thermal conductivities of the NWs accurately as well as experimental studies had been carried out.[163,164] Hou et al.[165] developed a comprehensive analytical solution including the NW-substrate interaction and radiation heat loss. Their study showed that for NWs with a diameter around 100 nm or thinner, the radiation heat loss from the wire surface would have a strong effect on the amplitude and phase shift of the 3ω signal.[165] This influence became stronger for thinner NWs. More importantly, from the mechanism of this 3ω method, the samples were required to be electrical conductive and have linear *I-V* behaviors within the source range. Besides, the TCR of the NW had to be known,which needed to be measured separately.

RSC Advances Accepted Manuscript

III-2.4 Applications

The 3ω method, coined by Corbino et al.[166] in 1910, was based on the discovered small third-harmonic voltage component while applying an ac current with angular modulation frequency, ω, through a heater. Later, this method was systematic investigated and became practical.[167-170] Theoretical analysis showed that the thermal parameters could be obtained by measuring the third harmonic component (3ω) of the voltage along a heating wire.[171] Lu et al.[69] further extended the 3ω method to simultaneously measure the specific heat and thermal conductivity of suspended fiber samples across two heat sinks, and, therefore, gave a relatively better SNR. Previously, it was mainly used to study the thermophysical properties of thin film,[167,172-178] superlattices,[179,180] and even liquid materials.[170,181,182]

As for 1D nanostructural materials, this method had also been utilized to investigate the thermal properties of NWs[62,183-188] CNTs,[189,190] and fibers.[159,191] Lee et al.[62] fabricated a measurement platform with nanoscale four-point setup, as shown in Fig. 6(b), for characterizing the thermoelectric properties of individual β-SiC NW and utilized the 3ω method to obtain the thermal conductivity of the NW. The 3ω voltage as a function of current at 1 kHz was measured, from which the thermal conductivity of 86.5 ± 3.5 W/mK was obtained at room temperature. Similarly, Choi et al.[189] found the thermal conductivity of individual MWCNTs (outer diameter of 45 nm), by employing the 3ω method, to be 650–830 W/mK at room temperature. Furthermore, Finefrock et al.[159] measured the thermal conductivity of PbTe nanocrystal coated glass fibers using the self-heated 3ω method at low frequency. They also performed a simulation to correct the thermal radiation effect and extract the thermal conductivities of glass fibers which were in the range of 0.50−0.93 W/mK near room temperature.

Recently, Dames et al.[164] pointed out that, with an additional dc offset, the thermal conductivity could also be determined from 1ω and 2ω voltages. Feng et al.[192] based on the numerical solution of heat conduction equation, presented an approach to measure the thermal properties of NWs with 2ω or 3ω voltage. This approach was also used to investigate a single Pt NW and carbon fiber and the result had a relative derivation within 4% using either 2ω or 3ω method. However, the 3ω measurement was still superior, despite that the 2ω method was able to yield a larger harmonic signal, relatively, than 2ω method. [164,192] Recently, Xing et al.[193] presented a complete model for characterizing the thermal properties of the NWs. With this 3ω technique, they also carried out a measurement of Pt NW as a reference sample using both voltage and current sources for sample excitation.[191] In particular, a first harmonic (1ω) cancellation technique was developed, in their work, to measure all the relevant thermal properties independently and also improved the measurement precision. It was also observed that the mesoscopic device, which was mentioned in section 2.1 and employed to measure the Seebeck coefficient, had a similar structure with the structure in the 3ω method. Therefore, the mesoscopic device could be also used to perform the 3ω measurement, thus to obtain the figure of merit ZT. For example, Lee et al.[194] provided a platform with built-in heaters and electrodes to measure electrical resistivity, thermal conductivity, and Seebeck coefficient simultaneously. The result showed that the thermal conductivity of a single crystalline $Bi_{1.75}Sb_{0.25}Te_{2.02}$ NW of 250 nm in diameter increased from 0.5 W/mK at 10 K to 1.2 W/mK at 120 K, then followed by a slight increase to 1.4 W/mK at 300 K. In literature [185], the three thermoelectric related properties of Bi_2Te_3 NWs were also successfully measured using this versatile microfabrication approach.

RSC Advances Accepted Manuscript

III-3 T-type nanosensor

III-3.1 Structure

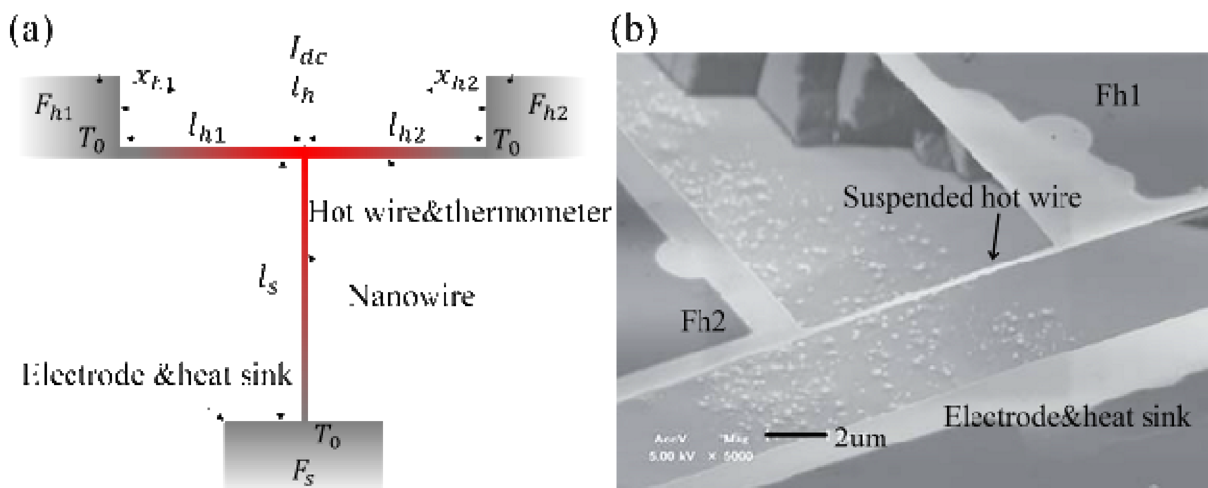

Fig. 7 (a) Schematic diagram of T-type nanosensor, in which the NW is attached a hot wire at one end and a heat sink at another end; (b) SEM image of the T-type nanosensor with suspended hot wire. Reprinted with permission from ref. 195, John Wiley and Sons.

Zhang et al.[196] developed a steady-state short-hot-wire method, in which a sample-attached T-type nanosensor was fabricated to measure the thermal conductivity of a single NW. The measuring system was schematically showed in Fig. 7(a). The hot wire of length l_h, radius r_h and thermal conductivity κ_h was suspended by two electric contacts, F_{h1} and F_{h2}, which also severed as heat sinks, at each end. The sample of length l_s and radius r_s was supported with a another electric contact, (F_s) at one end, and the other end was attached to the hot wire in the mid-point. The lengths between the attached point and left/right (F_{h1}/F_{h2}) heat sinks were l_{h1} and l_{h2}, respectively.

III-3.2 Principle

Once a constant direct current, I_{dc}, passed through the hot wire, a uniform Joule heat was generated, and during the entire measurement, all the ends connected with the heat sinks were maintained at the initial temperature,T_0. What's more, the temperature of the hot wire and the sample depended on their thermal properties and the heat generation rate of the hot wire. With the solutions of one-dimensional steady-state heat conduction along the hot wire and the sample, one could obtain the thermal conductivity of the sample by measuring the average temperature of the hot wire and calculating the heat generation rate. This method was theoretically applicable to any kind of individual nanofiber and NW.[197,198]

Assuming the heat loss was neglected when the measurement was carried out in a vacuum, and the effect of radiation was also neglected because of the small temperature gradient along the hot wire. Furthermore, the thermal resistance of the contact was also ignored in order to simplify this model. Then, the relevant one-dimensional heat conduction equations of hot wire could be expressed as[199]

RSC Advances Accepted Manuscript

$$\kappa_h \frac{d^2 T_{h1}(x_{h1})}{dx_{h1}^2} + q_v = 0$$
$$\kappa_h \frac{d^2 T_{h2}(x_{h2})}{dx_{h2}^2} + q_v = 0 \tag{3-9}$$

where $T_{h1}(x_{h1})$ and $T_{h2}(x_{h2})$ are the temperature at x_{h1} and x_{h2}, respectively. κ_h is the thermal conductivity of the hot wire, and q_v, defined as $IV/(A_h l_h)$, is the volumetric heat generation rate, where I,V and A_h are the supplied electrical current, the voltage and the cross area of hot wire, respectively.

As for the sample, the equation of heat conduction could be written as

$$\kappa_s \frac{dT_s(x_s)}{dx_s^2} = 0 \tag{3-10}$$

where $T_s(x_s)$ is the temperature of the sample at x_s, and κ_s is the thermal conductivity of the sample.

Under the boundary condition, that was, the temperatures of the heat sinks were the same as the surrounding temperature, T_0, and the temperature of the contact point between the hot wire and the sample is T_c, the equations (3-9) and (3-10) could be solved. Then, the average temperature rise of the hot wire could be calculated as

$$\Delta T_h = \frac{1}{l_h}\int_0^{l_h} T(x) - T_0 dx = \frac{l_{h1}^3 + l_{h2}^3}{12\kappa_h} q_v + \frac{T_c - T_0}{2} \tag{3-11}$$

Next, the heat flow through the NW was obtained as

$$q_s = -\kappa_h \frac{A_h}{A_s}\left(\frac{\partial T_{h1}}{\partial x_{h1}} + \frac{\partial T_{h2}}{\partial x_{h2}}\right) = \kappa_h l_h \frac{A_h}{A_s}\left(\frac{q_v}{2\kappa_h} - \frac{(T_c - T_0)}{l_{h1} l_{h2}}\right) \tag{3-12}$$

where A_s is the cross area of sample. Considering the temperature gradient of the sample, the heat flux of NW could be also expressed as

$$q_s = \kappa_s \frac{T_c - T_0}{l_s} \tag{3-13}$$

Combining (3-11), (3-12) and (3-13), the thermal conductivity of the NW was[199]

$$\kappa_s = \frac{l_s l_h^4 \kappa_h A_h q_v - 12 l_s l_h^2 \kappa_h^2 A_h \Delta T_h}{12 l_{h1} l_{h2} A_s l_h \kappa_h \Delta T_h - \left(l_{h1}^3 + l_{h2}^3\right) l_{h1} l_{h2} A_s q_v} \tag{3-14}$$

In principle, steady state was reached within several seconds when the constant direct current passes through the hot wire. As long as the ΔT_h and q_v were measured, one could obtain the thermal conductivity κ_s.

III-3.3 Merits and shortages

RSC Advances Accepted Manuscript

This method was, in principle, able to characterize the thermal properties of any single nanofiber, NW, and even SWCNT. It was regarded as having the advantages of simplicity as well as high accuracy. For example, uncertainty analysis was calculated, including uncertainty of hot wire thermal conductivity, thermal contact resistance and etc., to be within 7%, which was accepted as high accuracy.[196,199] In additional, the junction thermal contact resistance could be theoretically extracted through changing the length of the sample.[195] However, it was difficult to be applied in experiments at the nanoscale. The error caused by thermal contact resistance was depending on the contact length and can be as large as 20%, which indicated that the thermal contact resistance had a significant effect on this measurement and, to a large extent, limited its reliability and accuracy.[199] Futhermore, the hot wire must be fabricated at nanoscale to acquire sufficient sensitivity when measuring NWs. The connection between the hot wire and NW also became one of the fundamental points of this measurement which had been verified by Ito et al..[195,199] By bonding the Pt hot wire and the NW to make the contact length equal to the width of the Pt hot wire, the deviation of the measured thermal conductivities between considering the thermal resistance and the case without considering the thermal resistance was reduced.

III-3.4 Applications

This method had been successfully applied to measure the thermal conductivity of CNTs[197,198] and other NWs.[199,200] Fujii et al.,[195] fabricated suspended platinum nanofilm and lead terminals using a micro-electro-mechanical system (MEMS) technology. As illustrated in Fig. 7(b), the dimensions of the nanofilm were 27.5–40.0 nm in thickness, 330–600 nm in width, and 5.3–5.7 μm in length, respectively. The nanofilm was suspended about 6 μm above the silicon substrate and served as the hot wire. With this platform, it was found that the thermal conductivity of a CNT with a diameter of 9.8 nm was exceeded 2000W/mK at the room temperature. In additional, they also found that the thermal conductivity increased as its diameter decreases, which was contrary to many other 1D nanostructural thermoelectric materials.[99,103] Ito et al.[199] characterized the thermal conductivity of SiC NW with a diamante of 141 nm. The measurement result was obtained, in which the thermal conductivity turned out to be approximately 110W/mK at 300k. Furthermore, a 3ω-T type probe was proposed to measure the thermal properties of NWs and the thermal contact resistance of the junction.[201,202] More interestingly, a T-type probe composed of Wollaston wire was further developed in both 1ω and 3ω configurations for thermal conductivity measurements,[203,204] which was very conceptually similar to that of Fujii et al..[198]

III-4 Steady-state dc thermal bridge method (DCTBM)

III-4.1 Structure

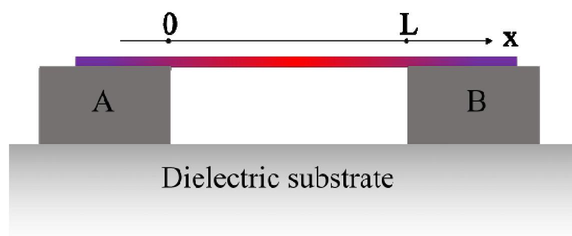

Fig. 8 Structure of the DCTBM for 1D nanostructure thermal conductivity measurement.

RSC Advances Accepted Manuscript

The structural scheme of the DCTBM was shown in Fig. 8, where the NW was suspended between two electrodes, A and B, which also served as heat sinks.

III-4.2 Principle

The sample, suspended over the two heat sinks, was heated at a steady state when a dc current passed through. Then, the resistance changed correspondingly, which was recorded using a four-prob technology. The temperature distribution could be determined according to one-dimensional heat conduction and the boundary conditions $T(x=0)=T(x=L)=T_0$, in which T_0 was the ambient temperature,[124]

$$T = T_0 + \frac{VI}{2\kappa A}x - \frac{VI}{2\kappa L A_S}x^2 \tag{3-15}$$

where κ,V, I, L and A_S are the thermal conductivity, the voltage, the current, the effective length and the cross section of the sample, respectively. The average temperature rise, then, was expressed as[124]

$$\Delta T = \frac{VIL}{12\kappa A_S} \tag{3-16}$$

Therefore, the thermal conductivity could be determined as long as the heating power, the corresponding temperature rise and NW's geometric parameters were acquired.

To measure the thermal conductivity accurately, the sample had to place in a vacuum chamber in order to reduce the heat loss due to air convection. In additional, the resistance-temperature relationship, which was used to determine the temperature, needed to be calibrated before the measurement of thermal conductivity.

III-4.3 Merits and shortages

This method could be utilized to evaluate both conductive and nonconductive samples. For conductive materials, the sample could serve as both a heater and a thermometer; for nonconductive samples, one might deposit an additional metallic coating on the sample to act as the heater and thermometer. For example, Pt was selected as the coating layer on individual poly(ether ketone) (PEK)/CNT fibers because of its stable temperature-resistance relationship and lower thermal conductivity (compared with Au).[124] However, it was necessary to extract the real thermal conductivity of sample from the results with metallic coating. The effect of metallic coating should also be considered. Additionally, up to date, only large fibers (>15μm) had been measured by this method. When applying to NWs, the effect of the thermal contact resistance and radiation heat loss needed to be evaluated before the measurement.

III-4.4 Applications

Moon et al.[124] developed the DCTBM and measured the thermal conductivity of individual poly(ether ketone) (PEK)/CNT composite fibers over a temperature range of 295–400K. The thermal conductivities of those fibers at 390 K were found to be about 27 W/mK, which was comparable to some engineering alloys. Moreover, the thermal conductivity of multi-wall CNTs (MWCNTs) containing Bi-component fibers were also measured, using this measuring method, to be approximately 7 W/mK.[205]

RSC Advances Accepted Manuscript

III-5 Optical heating and electrical thermal sensing (OHETS)

III-5.1 Structure

In this method, the sample was suspended over two electrodes, A and B, as shown in Fig. 8. Futhermore, a periodically modulated laser beam was employed to irradiate the sample.

III-5.2 Principle

When the sample was irradiated using a periodically modulated laser beam, it would experience a periodical temperature change with time owing to the periodical laser heating, which, as a result, would lead to a periodical change in its electrical resistance.

A small dc current was applied through the electrodes, A and B, to detect the voltage variation which had the same frequency with the modulated laser beam. Additionally, the voltage variation was strongly affected by the heat conduction along the NW. Therefore, the thermophysical properties of the sample could be determined through the phase shift of the voltage variation relative to the laser beam.

The NW was assumed to have a uniform temperature distribution in its cross-section, as long as the thermal diffusion length, $\mu=\sqrt{(2\alpha/\omega)}$ (α: thermal diffusivity of the wire; ω: modulation frequency), was much larger than the sample diameter D. Furthermore, to enhance the effect of the heat sinks, dimensions of the heat sinks needed to be much larger than the diameter of the sample. This resulted in negligible temperature variation at the heat sinks due to the laser heating.

When the laser heating power had the form of $I=I_0(1+\cos(\omega t)/2)$, the heat transfer equation along the axial direction of the NW could be written as[206]

$$\frac{\partial\left(\rho c_p T\right)}{\partial t}=\kappa\frac{\partial^2 T}{\partial z^2}+Q_0 e^{i\omega t}+Q_0 \qquad (3\text{-}17)$$

where $Q_0=E/LA_s$, E and A_s are laser beam energy absorbed by the sample and cross-sectional area of the wire, respectively. c_p, κ and ρ are the specific heat, the thermal conductivity and the density of the sample, respectively. Moreover, the laser beam was assumed to be uniform over the sample. Thus the effect of nonuniform distribution of the laser beam could be neglected.[206]

In this method, a lock-in amplifier could only detect the temperature component that periodically varied with time ($\tilde{T}_s$), which was in the form of $\tilde{T}_s=\theta e^{i\omega t}$, in which θ is the temperature of the NW. Then, the average temperature variation ($\bar{\tilde{T}}_s$) along the wire was expressed as

$$\bar{\tilde{\mathrm{T}}}_s=\bar{\theta}e^{i\omega t}=\bar{\theta}_0^{\,i(\omega t+\phi)} \qquad (3\text{-}18)$$

where $\bar{\theta}_0$ and ϕ are the amplitude and phase of $\bar{\theta}$, respectively. Therefore, using the real part of $\bar{\tilde{T}}_s$, the ω voltage across the NW was[206]

$$V_\omega=\bar{\theta}_0\frac{dR}{dT}I\cdot\cos\left(\omega t+\phi\right) \qquad (3\text{-}19)$$

RSC Advances Accepted Manuscript

Equation (3-19) implied that, in this method, the phase shift of the voltage variation over the NW should be measured and be used for data fitting. In other words, once the phase shift as a function of the modulation frequency for the sample was measured, the thermal diffusivity could be determined by data fitting.

III-5.3 Merits and shortages

The OHETS method could be used to characterize the thermal properties of 1D conductive and nonconductive NWs. It was also noted that the nonuniformity of the laser beam distribution and the radiation heat loss from the sample, which was housed in a vacuum chamber, had negligible effect on the measured phase shift.[207] However, an additional metallic coating needed to be deposited on the sample for nonconductive NWs. As the diameter of the wire was reduced in this method, the metallic coating would have a considerable contribution to the heat conduction.[206] The effect of metallic coating should be considered and the real thermal property of the sample needed to be extracted. Besides, the thermal diffusivity of the sample was measured rather than the thermal conductivity. The material's density and specific heat were required to calculate the thermal conductivity. Yet, these two parameters were mostly extracted from the bulk counterpart. Furthermore, the system time delay had to be calibrated, before carrying out this method, by detecting the phase shift between the synchronizing signal of the function generator and the modulated laser beam.[206]

III-5.4 Applications

Hou et al.[206] developed this OHETS method and measured the thermal diffusivity of conductive SWCNTs bundles. By fitting the measured phase shift of the voltage variation over the NW, the measured thermal diffusivities of the SWCNT bundles were obtained in ranges of $2.98\sim6.54\times10^{-5}$ m^2s^{-1}. In additional, applying this method, the thermal diffusivity of single nonconductive polyacrylonitrile (PAN) fibers(~800nm) were characterized to be $1.05\sim1.14\times10^{-5}$ m^2s^{-1}.[207]

III-6 Transient electrothermal method (TET)

III-6.1 Structure

The schematic structure of the TET method was illustrated in Fig. 8, in which the NW was suspended between two electrodes, A and B.

III-6.2 Principle

In this method, the to-be-measured NW was suspended over two electrodes as shown in Fig. 8. When the sample was fed with a dc current which introduced electrical heating from electrodes A, B, the temperature change of the sample would lead to its resistance change, which could be detected by measuring the voltage change of the sample. In additional, the temperature increasing history of the sample was strongly affected by the heat transfer along it. Therefore, the thermal diffusivity of the sample could be measured by fitting the temperature change curve against time.

RSC Advances Accepted Manuscript

When the heating power was generated due to the dc current, the heat transfer equation in the NW along the x direction at time t>0 was written as

$$\frac{\partial(\rho c_p T)}{\partial t} = \kappa \frac{\partial^2 T}{\partial x^2} + q_0 \qquad (3\text{-}20)$$

where q_0, κ, c_p and ρ are the electrical heating power per unit volume, the thermal conductivity, specific heat and density of the sample, respectively.

Considering the initial condition, T(x,t=0) = T_0, and the boundary conditions, T(x=0,t) = T(x=L,t) = T_0, where T_0 and L are the ambient temperature and the length of the wire, the average temperature of the wire can be written as

$$\begin{aligned} T(t) &= \frac{1}{L}\int_{x=0}^{L} T(x,t)dx \\ &= T_0 + \frac{8q_0L^2}{\kappa\pi^4}\sum_{m=1}^{\infty}\frac{1-\exp\left[-(2m-1)^2\pi^2\alpha t/L^2\right]}{(2m-1)^4} \end{aligned} \qquad (3\text{-}21)$$

where α is the thermal diffusivity of the sample.

The temperature distribution would finally reach the steady state and the average temperature of the sample was

$$T(t\to\infty) = T_0 + \frac{q_0L^2}{12\kappa} \qquad (3\text{-}22)$$

Therefore, the normalized temperature rise could be expressed as[123]

$$\begin{aligned} T^* &= \left[T(t)-T_0\right]/\left[T(t\to\infty)-T_0\right] \\ &= \frac{96}{\pi^4}\sum_{m=1}^{\infty}\frac{1-\exp\left[-(2m-1)^2\pi^2\alpha t/L^2\right]}{(2m-1)^4} \end{aligned} \qquad (3\text{-}23)$$

where α, T_0, T(t), T(t→∞) are the thermal diffusivity of the sample, ambient temperature, average temperature of the NW at time t and steady state, respectively.

It was noted that, from equation (3-23), the shape of the normalized temperature rise was only related to the Fourier number, which defined as $F_0=\alpha t/L^2$, for any kinds of materials.

There were three methods for data analysis to determine the thermal diffusivity:[123]

i) Linear fitting at the initial stage of electrical heating

At the beginning of of the electrical heating, 0<t<Δt, the corresponding normalized temperature rise was written as

$$T^* = 12\alpha / L^2 \Delta t \qquad (3\text{-}24)$$

Using the NW's length, the thermal diffusivity, α, could be determined from the slope of the normalized temperature increasing curve.

ii) Characteristic point method

One best characteristic point of the T~t curve, could be used to obtain the thermal diffusivity directly, when T*=0.8665, and the corresponding Fourier number was 0.2026. Therefore, the thermal diffusivity of the sample was expressed as

$$\alpha = 0.2026L^2 / \Delta t_c \qquad (3\text{-}25)$$

RSC Advances Accepted Manuscript

iii) Least square fitting method

Using different trial values of the thermal diffusivity, the best thermal diffusivity could be found by employing global fitting of the experimental data.

III-6.3 Merits and shortages

The TET method was a rapid technique (within few seconds) that could be applied to nonconductive samples. Compared with the 3ω and OHETS methods, this method featured much reduced measurement time and much stronger signal level. Another merit was that an estimation of the thermal contact resistance in this method was unnecessary.[70] However, when this method was applied to nonconductive NW by applying a thin metallic coating on the top of the sample, it added significant complexity to the measurement. More importantly, the additional metallic coating on the sample would undoubtedly increase the measurement difficulty when applying this method to NW with small diameter (e.g. 10nm). Besides, the analytical expression of the normalized temperature evolution was only suitable for the issues with a constant heating power.[208] Potential errors would be introduced with nonconstant heating power due to the variation of sample resistance. For example, supposing that a constant voltage was supplied and the resistance of the sample increased as a result of self-heating, the current through it would decrease, leading to more steady heating power over the sample. The deviation for thermal conductivity, originating from the heating power variation had been accounted to be around 10% for 10 μm thick Pt wire.[208] However, connecting a resistor with the same resistance as the sample in series or parallel would decrease the heating power fluctuation to less than 4%. Another issue in this method was that it was difficult to implement the measurement when the characteristic time of heat transfer of the sample was comparable to or less than the rising time of the electric current.[209,210] Consider a NW with thermal diffusivity of $\sim5\times10^{-5}$ m^2s^{-1} (e.g. CNTs) and length ~1um, the characteristic time of heat transfer would be 2×10^{-2} μs. Yet, the rising time of the electric current was ~2μs in ref. 211 which was much greater than the given characteristic time of heat transfer. Consequently, this method was limited by the rising time of the electric current. It was also worth noting that this method was aimed at measuring the thermal diffusivity. To obtain the thermal conductivity, one had to estimate or measure the density and the heat capacity of the sample, thus the actual thermal conductivity could be calculated.

III-6.4 Applications

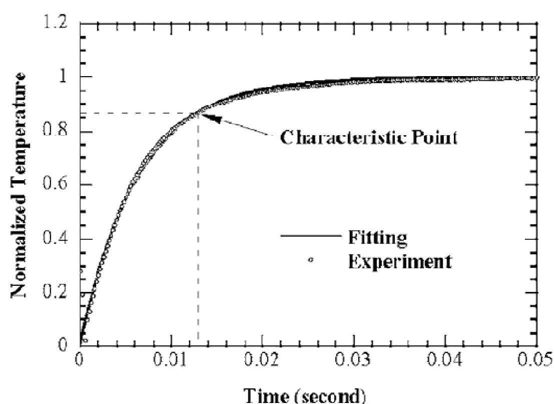

Fig. 9 The normalized temperature vs the theoretical fitting for the SWCNT bundle. Reprinted with permission from ref. 123, AIP Publishing LLC.

RSC Advances Accepted Manuscript

The TET technique was an effective method to assess the thermal diffusivity of materials, including conductive, semiconductive and nonconductive low-dimensional structures. This technique had been used for measuring the thermal diffusivity of thin films composed of anatase TiO_2 nanofibers,[212] free-standing micrometer-thick Poly (3-hexylthiophene) films,[213] SWCNTs[214] and micro/submicroscale polyacrylonitrile wires[211] successfully.

Guo et al.[123] outlined this measurement to measure the thermophysical properties of one-dimensional conductive and nonconductive NWs. Their uncertainty analysis showed that the experiment had an uncertainty more than 10%. Moreover, the average thermal diffusivities of SWCNT bundles was obtained from Fig. 9, which was found to be $1.15\times10^{-5}m^2s^{-1}$. Using this method, the thermal diffusivity of SWCNT bundles was also found at 10^{-5} level which was the same as that in literature [214]. In additional, development and analysis of this method had been also carried out. Feng et al.[208] developed this method to simultaneously measure the specific heat and the thermal conductivity of individual samples, and the accuracies of both the measurements were less than 6%. Very recently, Liu et al.[215] analyzed the TET technique and found the TET technique was an effective approach to measuring the thermal properties of various materials. Computational models were also developed for the anisotropic thermal characterization of multi-scale wires.[216] In additional, a full theoretical model of the TET method had also been derived to include the effects of radiation heat transfer and non-constant heating.[217]

III-7 Transient photoelectrothermal (TPET) technique

III-7.1 Structure

In this measurement, the measuring NW was suspended over two metallic electrodes, as shown in Fig. 8, and irradiated with a step cw laser beam.

III-7.2 Principle

The NW was suspended over two metallic electrodes, as shown in Fig. 8. Furthermore, it was irradiated by a step cw laser beam, and the laser spot should be large enough so as to cover the entire NW and portion of the electrodes. The laser beam would induce a transient temperature rise in the NW, and then resulted in a transient variation of the electrical resistance of the sample. The temperature variation amplitude of the electrodes (also as huge heat sinks), was much smaller than that of the NW. This ensured that the resistance variation of the electrodes was negligible compared with that of the sample. To extract the thermophysical properties of the NW, a dc current needed to be applied from the two electrodes, A and B, and the transient voltage variation of the NW should be detected.

Assuming that the temperature distribution in the cross section of the NW was uniform, therefore, only the heat transfer in the axial direction of the sample needed to be considered. If the output power of the laser was maintained constant, the heat transfer equation along the NW was[218]

$$\frac{\partial\left(\rho c_p T\right)}{\partial t} = \kappa \frac{\partial^2 T}{\partial x^2} + \left(\dot{g} + g'\right) \qquad (3\text{-}26)$$

RSC Advances Accepted Manuscript

where $\dot{g}$ and g', defined as heating power per cubic meter, are the heat generated by the laser beam and the direct current passing through the sample, respectively. κ, c_p, ρ and T are the thermal conductivity, specific heat, density and temperature of the sample, respectively.

Following the same derivation process of TET method, the normalized average temperature rise could be expressed as[218]

$$T^* = 96\sum_{m=1}^{\infty}\frac{1-\exp\left[-\left(2m-1\right)^2\pi^2\alpha t/L^2\right]}{\left(2m-1\right)^4} \qquad (3\text{-}27)$$

Considering the temperature, resistance change and voltage variation relationship of the wire, the measured voltage variation could represent the evolution of the normalized temperature. Consequently, according to the normalized temperature evolution, the thermal diffusivity could be determined by the data analysis methods which have been previously mentioned in the TET method.

III-7.3 Merits and shortages

The TPET method was developed to measure the thermal diffusivity of materials, including conductive, semiconductive and nonconductive low-dimensional structures based on step laser heating and electrical thermal sensing. It featured a strong signal and took only few seconds. In the experiment, only the information about how fast the voltage increased to reach steady state was needed. No knowledge about the real temperature rise was required.[218] However, noting that this method had only been applied to wires with diameter about 10um, several essential issues deserved careful technical consideration when the NWs were measured. First, just as the TET method, this method faced the issue that the rising time of the laser beam might be comparable to or greater than the time taken for the sample to reach steady state. To make the effect of rising time of the laser beam negligible, fast optical switches to control the laser beam might be used.[218] Second, for nonconductive NWs, the thickness of the metallic coating would be comparable to the NW thickness, which could introduce considerable errors. Other technologies, such as Raman spectrum, might be required to solve this problem. Third, theoretical analysis for the effect of radiation heat loss was recommended when NW was measured. What's more, this method could only measure the thermal diffusivity. The material's density and specific heat were required to calculate the thermal conductivity.

III-7.4 Applications

Wang et al.[218] developed this measurement to measure the thermophysical properties of conductive and nonconductive wires. They had successfully characterized the thermal diffusivities of a SWCNT bundle and microscale nonconductive wires. As a result, the thermal diffusivity of the SWCNT bundle was measured to be $2.53\times10^{-5}m^2s^{-1}$, which was much smaller than that of graphite in the layer direction.

III-8 Pulse Laser-assisted Thermal Relaxation (PLTR) Technique

III-8.1 Structure

RSC Advances Accepted Manuscript

The measuring NW was suspended over two metallic electrodes, A and B, which acted as both contacts and heat sinks, as illustrated in Fig. 8, and irradiated by a fast pulsed laser.

III-8.2 **Principle**

Upon fast (nanosecond) pulsed laser irradiation, the temperature of the sample would suddenly increase to a high level and then went down gradually. Such temperature relaxation was strongly affected by the thermal diffusivity and the length of the NW. In order to record this temperature relaxation history, a small direct current was fed through the electrodes, A and B, to obtain its resistance change which corresponded with the temperature change. Consequently, the shape of the normalized $\Delta V \sim t$ cure, which shared the same shape as the $\Delta T \sim t$ cure, could be used to obtain the thermal diffusivity of the sample.

The heat transfer equation in the NW along the x direction at time t>0 was the same as equation (3-20). However, here q_0 is sum of the Joule heating and the laser pulse heating. Since temperature evolution was caused by the pulsed laser heating, the effect of the Joule heating was not concerned. With homogeneous boundary conditions, $T(x=0,t)=T(x=L,t)=T_0$, and initial conditions, $T(x,t=0)=T_0$, where T_0 and L are the ambient temperature and the length of the NW, and following the same derivation process of TET method, the simplified and normalized temperature relaxation could be written as[209]

$$T^* = \frac{8}{\pi^2} \sum_{m=1}^{\infty} \frac{\exp\left[-(2m-1)^2 \pi^2 \alpha t / L^2\right]}{(2m-1)^2} \qquad (3\text{-}28)$$

Equation (3-28) showed that the shape of the normalized temperature relaxation was only effected by the Fourier number $F_0=\alpha t/L^2$.

To determine the thermal diffusivity, two approaches were involved: characteristic point method and global data fitting of the temperature relaxation curve which have been previously mentioned in the TET method.

III-8.3 **Merits and shortages**

This method could be employed to characterize the thermal properties of one-dimensional micro conductive and nonconductive wires. It was noted that this PLTR technique was the development of the TET and TPET method. The laser heating time could be as short as $\sim 10^{-9}$ s which was much less than the characteristic time of heat transfer of most samples. Consequently, it could be used to determine the thermal diffusivities of wires which had relatively short characteristic times of heat transfer (e.g. 10^{-8} s) and surmounted the drawbacks of the TET and TPET techniques while providing comparable reduced experimental time and high signal/noise ratio.[209] Nevertheless, this method had been only applied to wires with diameter about 20um, careful technical considerations were needed when the NWs were measured, such as the radiation heat transfer and the influence of metallic coating, which have been discussed previously. Additionally, another issue was that, when the thermal conductivity of the sample was much higher than that of the electrodes, the temperature at the wire/electrode contacts might not be actually fixed at the ambient temperature.[209] Additional deposition of other metallic material on the contact area might be required.

III-8.4 **Applications**

RSC Advances Accepted Manuscript

This method overcame the drawbacks of the TET and TPET techniques and the analyzed uncertainty of this measurement was less than 10%.[125] Guo et al.,[209] using this method, measured the thermal diffusivity of a MWCNT which was calculated to be $1.46\times10^{-5}m^2s^{-1}$, and the measured average thermal diffusivity of carbon fibers was $9.9\times10^{-5}m^2s^{-1}$. Recently, a theoretical analysis of the PLTR technique based on a finite difference model, which involved anisotropic heat transfer and radiation heat lost to the surroundings, had been developed.[210] Using this validated model, the heat transfer characteristics of multiscale wires including CNT had been studied.

III-9 Measurements by Raman Thermography

III-9.1Structure

In this method the sample was suspended over a trench, and the four electrodes (A,B,C and D) worked as both contacts and heat sinks which was shown in Fig. 6(a).

III-9.2 Principle

It was worth mentioning that there were several models involving the Raman Thermography. One of the measurements adopting Raman Thermography was steady-state Joule heating and optical sensing.[219,220] When there was a direct current passing through the NW, the sample heated itself. The temperature gradient between the middle and each end of the NW was strongly affected by its intrinsic heat transfer capability. Therefore, the thermal conductivity could be determined by figuring out the relationship between the heating power and the temperature difference over the middle and the two ends of the NW.

The heat power, P, generated on the section could be calculated as the volume integral on heat power density (Wm^{-3}), ρ_h,

$$P = U \times I = \int_V \rho_h dV \tag{3-29}$$

where U and V are the voltage and the volume of the effect section of the sample, respectively.

When the sample was in a vacuum, the infrared radiation was neglected. The majority of the generated heat was conducted through the suspended NW to the substrates which acted as heat sinks. When the system reached its steady state, the whole generate heat was equal to the heat conducted away, that was

$$P = \int_{A_S} \vec{q} \cdot d\vec{A}_S = \int_V \left(\nabla \cdot \vec{q}\right) dV \tag{3-30}$$

where $\vec{q}$ is heat flux density in the unit of Wm^{-2}, and A_S is cross section of NW.

From equations (3-29) ,(3-30), and Fourier thermal transfer law, the following equation could be obtained:

$$\rho_h = -\kappa \times \frac{d^2T}{dx^2} \tag{3-31}$$

where κ is the thermal conductivity of the sample. The thermal power density ρ_h was approximately equal to UI/V, and V could be calculated as $V=A_SL$, where L is the length of the NW. Assuming the temperature of the heat sinks was the ambient temperature, T_0. The temperature at the mid point of the NW was T_h, which was the highest temperature along the wire. The thermal conductivity was determined as[220]

RSC Advances Accepted Manuscript

$$\kappa = \frac{UIL}{8S\times\left(T_h - T_0\right)} \tag{3-32}$$

Therefore, when the heat power, the geometric parameters of the sample and the temperature difference between the middle and end point of the NW were obtained, one could figure out the thermal conductivity. In additional, the temperature difference could be determined by the Raman spectra shift method.[221,222]

III-9.3 **Merits and shortages**

As described above, the thermal contact resistance was an unsolved key issue in determining the intrinsic thermal conductivity in most electrical measurement. Furthermore, it was difficult to obtain the concrete value of thermal contact resistance.[144,198,223] Comparing with that, the Raman Thermography was a noncontact temperature technology. It could avoid determining the temperature by the relationship between the temperature and resistance of the sample so to eliminate the influence of the thermal contact resistance. Yet, several issues should be considered in the experiment. On the one hand, a shift was existed between the laser focus position of the Raman spectrometer and the mid point of the sample due to the limited resolution of the Raman spectrometer. Supposing that the location shift was 10% of the total length, it would give about 4% uncertainty in the middle point temperature measurement.[219] On the other hand, the probing laser of the Raman spectrometer would heat the sample when measuring and induce a resistance variation of the sample. However, this variation was demonstrated to be negligible.[220] Another concern was that the temperature dependence of the Raman spectrum should be characterized and treated differently when different kinds of samples were analyzed.[219]

III-9.4 **Applications**

To date, several models had been developed using the Raman-thermal technique, to measure the thermal conductivity of fibers,[224] CNTs,[225] NWs,[226-228] and graphenes.[229,230] Yue et al.[219] measured the thermal conductivity of individual SWCNTs and MWNTs using the temperature-induced shifts of D band Raman spectra, and the value was measured to be 2400W/mK and 1400W/mK, respectively. Using the same model mentioned in this review, the thermal conductivities of MWCNT bundles were determined based on the temperature dependence intensity of the D band Raman shift peak, which was more sensitive than the shift of the G band.[225] Combining laser heating and Raman spectroscopy, Soini et al.[226] investigated the thermal properties of freely suspended GaAs NWs. The thermal conductivities of single 170 nm NWs were found to lie in the range of 8~36 W/mK. Hsu et al.[231] developed a model using optical heating and temperature detecting by temperature-induced shifts in the G band Raman frequency. But, owing to that it was difficult to ascertain the heat power generated by the laser, they did not give the concrete thermal conductivity. Doerk et al.[228] presented a model to measure the thermal conductivities of cantilevered NWs by heating with a focused laser locally, while simultaneously measuring the temperature of the same spot through Raman spectrometry. Very recently, combining Raman and electrical measurements, Wang et al.[232] developed a model to determine the optical absorption and heat transfer coefficients simultaneously. More interestingly, Li et al.[233] combining T-type with Raman measurements, successfully developed a noncontact T-type Raman spectroscopy method to measure the thermal conductivities of fibers which could easily eliminate the thermal contact resistance.

RSC Advances Accepted Manuscript

III-10 Thermal flash method

III-10.1 Structure

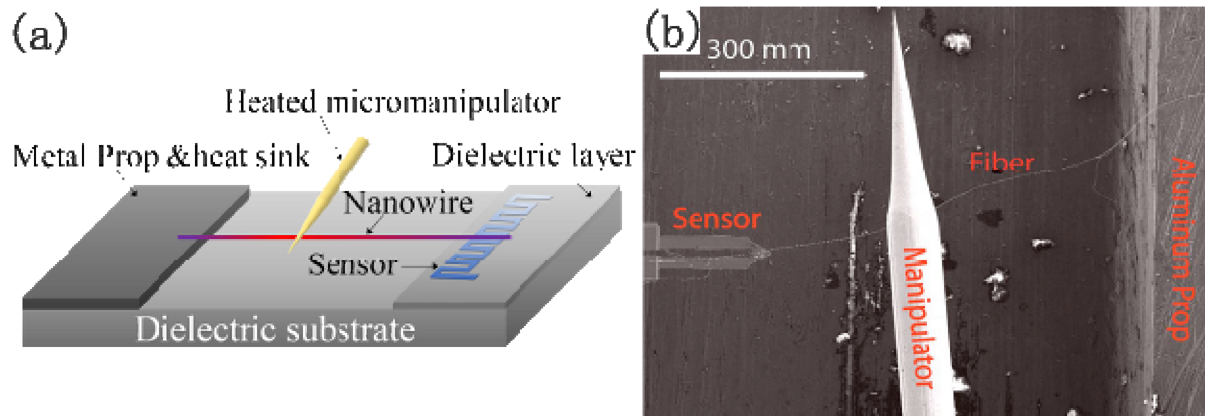

Fig. 10 (a) Schematic of the thermal flash method, in which the NW is suspended between the thermal sensor and a metallic prop; (b) A SEM image of the thermal flash measurement for a polyimide micro/nanofiber. Reprinted with permission from ref. 70, AIP Publishing LLC.

In this method, a test NW was positioned between the thermal sensor and a metallic prop acting as a heat sink which aimed to keep the sample suspended in vacuum, (see Fig. 10(a)). When implementing this method, a heat pulse would be sent into the sample from a micromanipulator based heater and then into the sensor.

III-10.2 Principle

This method was based on the thermal flash principle, which could direct characterize the thermal diffusivities of nanofibers without being influenced by the presence of interfacial or contact resistances.[70] In this method, a micromanipulator based heater was used to send a heat pulse through the NW and into the sensor. When the micromanipulator, which was wrapped with metal wire to sever as heater, contacted with the sample, heat would pass through the NW and then into the sensor. As a result, the resistance of the sensor would change and the transient voltage could be monitored while the sensor was maintained under a constant current.

The micromanipulator was modeled as a high temperature reservoir due to its relatively large size and high thermal conductivity compared with the sample. Thus, from the heat transfer equation, an analytical solution could be derived and applied to obtain the thermal diffusivity of the sample from the data measured. The normalized temporal variation of the temperature at the contact point between the sample and the sensor was derived as[70]

$$\overline{T}(t)=1+2\sum_{n=1}^{\infty}(-1)^n\, e^{\alpha_f n^2\pi^2 t/l_f} \qquad (3\text{-}33)$$

where α_f and l_f are thermal diffusivity and the length of the sample, respectively.

When applying this method, the time, t, was assumed to be equal to zero when the micromanipulator touched the sample. The sensor and the NW were modeled as being in perfect contact. Furthermore, equation (3-33) was a simplified expression due to the following equations

RSC Advances Accepted Manuscript

$$\frac{\kappa_s}{k_f}\sqrt{\frac{\alpha_f}{\alpha_s}} \gg 1 \quad \text{and} \quad \sqrt{\frac{\alpha_f}{\alpha_s}} \ll \frac{l_f}{l_s} \tag{3-34}$$

where κ,α and l are thermal conductivity, thermal diffusivity and length, respectively; the subscript f and s refer to the sample and the sensor, respectively. Equation (3-34) implied that the sample should be given with low thermal conductivity and sufficiently long length.

To obtain the thermal diffusivity, the equation (3-33), expression for the transient temperature rise of the sensor, could be utilized in a curve fitting routine as applied to the collected data. The thermal diffusivity of the sample could be determined from the best fitting between the analytical and experimental temperature profiles.

III-10.3 Merits and shortages

Since the transient variation was required to extract the thermal diffusivity rather than the magnitude of temperature, an offset due to thermal contact resistance, commonly a barrier to accurate thermal measurement, would not influence the final result.[70] However, since the measurement result was dependent on the sample thermal diffusivity and length, two main issues deserved careful technical consideration. On the one hand, the sample should be given with low thermal conductivity and sufficiently long length to satisfy the equation (3-34). Otherwise, more complex theoretical analysis should be implemented to solve this issue. On the other hand, the time taken to reach steady state was only few microseconds for fibers with relatively high thermal diffusivity, such as CNTs, since the exponential rise time was a function of both the thermal diffusivity and the length of the sample. For example, the time taken to reach steady state for MWNT clusters was approximately 8 μs.[126] Instrument with a fast data acquisition rate, such as a value in excess of 1×10^6 samples/s, was required. To solve this problem, up to 1 centimeter samples or digital oscilloscopes offering the maximum data acquisition rate of 1×10^6 samples/s were selected to meet the above requirements.[126,234] Additionally, this method measured thermal diffusivity rather than the thermal conductivity. The specific heat and density of the sample had to be known in order to properly report thermal conductivity values.

III-10.4 Applications

Demko et al.[70] developed this thermal flash method to characterize the low thermal diffusivity of nanofibers, as shown in Fig. 10(b). Their result showed that the polyimide fibers of diameters 570 and 271 nm exhibited diffusivities of $5.97\times10^{-8}m^2s^{-1}$ and $6.28\times10^{-8}m^2s^{-1}$, respectively. In additional, a comprehensive mathematical treatment and analysis of this thermal flash theory was also presented to measure the thermal diffusivity of nanostructures.[126,235] The analysis showed that this method can be carried out without calling for any knowledge or estimate of the interfacial/contact resistances. Recently, this method had also been utilized to measure the thermal conductivity of carbon nanofibers and graphene nanoplatelets[236,237] as well as polyimide-mesophase pitch nanofibers.[234]

III-11 Thermoreflectance Technique

III-11.1 Structure

RSC Advances Accepted Manuscript

The device, as shown in Fig. 2(a), consisted of two adjacent low-stress SiN_x membranes suspended with several beams. To prevent air convection influence on the thermal conductivity measurements, the sample was put in a cryostat chamber and kept in a high vacuum.

III-11.2 Principle

In this typical approach,[238] a direct current was applied to one of the suspended heater so that the heating power was generated and heater's average temperature was elevated above the ambient temperature. This power could be divided into two parts: heating up the active PRT, defined as Q_{active} and passing through the NW to heat up the inactive PRT, defined as $Q_{inactive}$. Furthermore, the heat conducted through the NW was assumed all pass to the inactive PRT side to heat it up. Thus, the following equation could be obtained[238]

$$IV = Q_{active} + Q_{inactive} \qquad (3\text{-}35)$$

At the same time, the heating power (Q) generated by PRT was expressed as

$$Q = G_l \Delta T \qquad (3\text{-}36)$$

where G_l and ΔT are the PRT thermal conductance and its temperature increase, respectively.

From equation (3-35) and (3-36), one could derive

$$IV = G_l(\Delta T_h + \Delta T_s) \qquad (3\text{-}37)$$

where ΔT_h andΔT_s are the temperature increase on the active and inactive PRT, respectively.

Then, the heat conducted through the NW was obtained as[238]

$$Q_{inactive} = \frac{\Delta T_s}{\Delta T_s + \Delta T_h} IV \qquad (3\text{-}38)$$

Consequently, the thermal conductivity could be calculated as

$$\kappa = G_N \frac{A_S}{l} = \frac{Q_{inactive}}{\Delta T_N}\frac{A_S}{l} \qquad (3\text{-}39)$$

where G_N, A_S, l and ΔT_N are thermal conductance, cross section, length and temperature difference of the NW, respectively.

To obtain ΔT, the thermoreflectance imaging technique was utilized, which was based on temperature dependence of the materials' reflection coefficient and able to provide lateral resolution of 0.3-0.5 μm and temperature resolution of 0.1 °C. In other words, a reflected light intensity change evoked by the temperature change was detected and turned into small electric signal. Therefore, the temperature increase and distributed could be obtained.

III-11.3 Merits and shortages

The thermoreflectance measurement was a noncontact temperature measuring method, which could achieve submicrometer spatial resolution and 0.1 °C temperature resolution.[238,239] In the experiment, the actual temperature distribution between the two electrodes where the NW bridged was directly measured, instead of the average temperature of the heater/sensor. No knowledge about the TCR of the heater was needed. Thus, an estimation of the thermal contact resistance in this method was unnecessary. Nonetheless, it was notable that the resolution of the thermoreflectance imaging technique was at submicrometer. Consequently, it was difficult to

RSC Advances Accepted Manuscript

apply this method to short NWs, the length of which was comparable to the spatial resolution. Another issue should be considered was that the thermoreflectance coefficient of the sample should be calibrated before the measurement, which was a time consuming process.

III-11.4 Applications

Zhang et al.[238] developed this method to characterize the heat transfer along a SiNW. They obtained thermoreflectance image of the NW and device and then calculated the thermal conductivity of the SiNW (115 nm in width and 3.9 μm in length) which was 46 W/mK. This value corresponded to the electrical measuring result, 40 W/mK, made by Li et al..[240]

III-12 3ω-Scanning Thermal Microscopy (SThM) Techniques

III-12.1 Structure

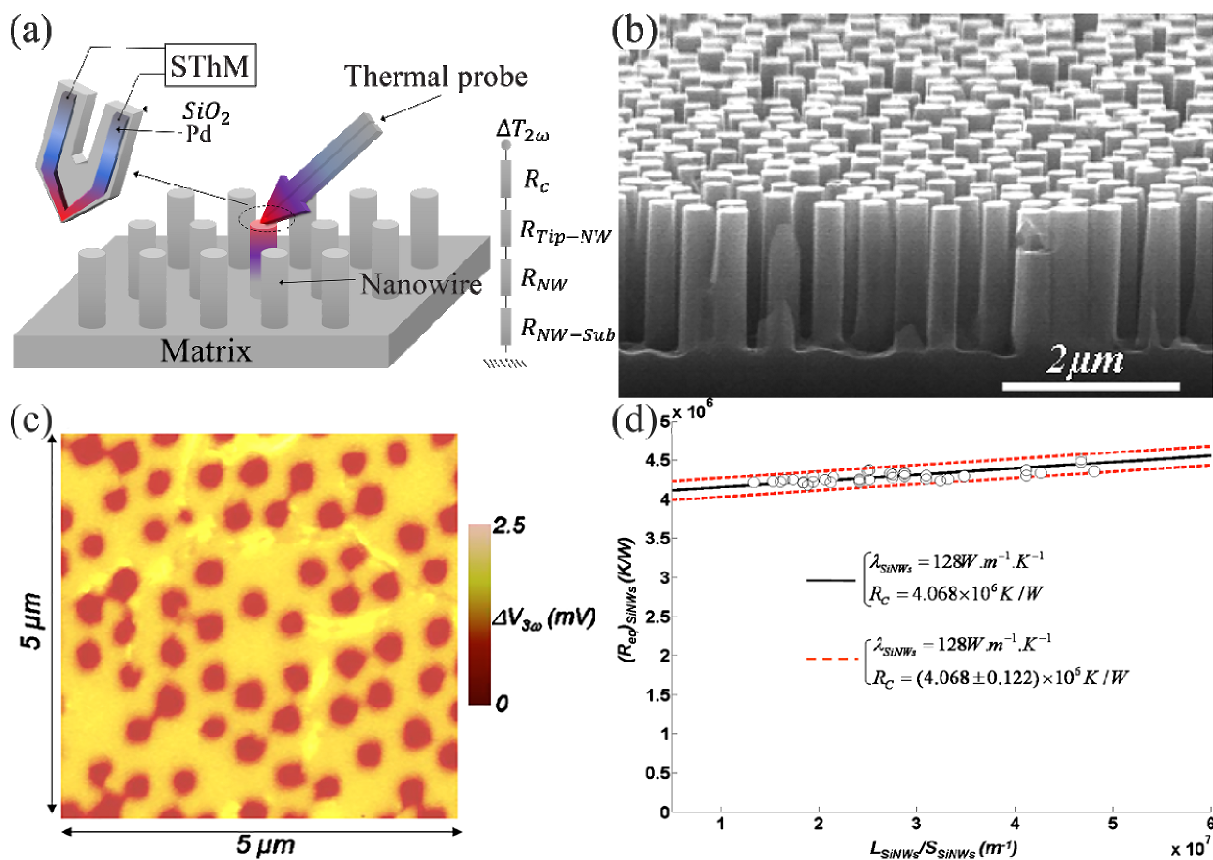

Fig. 11 (a) Schematic of SThM method for NW thermal conductivity measurement; (b) SEM pictures of the Si NWs array; (c) SThM thermal imaging of Si NWs embedded in a silica matrix; (d) Si NWs equivalent thermal resistance as a function of the ratio LNW/SNW: circles are used for experimental data and lines for the fits. Reprinted with permission from ref. 241, AIP Publishing LLC.

The schematic of SThM method for NW thermal conductivity measurement was shown in Fig. 11(a), where the tip was made of SiO_2 with a thin layer of palladium (Pd) deposited on the surface (top left of Fig. 11(a)). The Pd

RSC Advances Accepted Manuscript

strip played the role of a heater and a thermometer when this probe was in contact with the NW (mid of Fig. 11(a)).

III-12.2 Principle

Thermal measurements had been investigated using a 3ω SThM method in the early years, which was able to obtain both thermal images and contact mode topographical images.[242,243]

For the 3ω SThM measurement, a sinusoidal current $I(t)=I_0\sin(\omega t)$ passed through the thermoresistive probe, generating a Joule heat at pulsation 2ω. The resulting temperature variation $T_{2\omega}$ at the same pulsation then modulated the thermoresistive probe resistance at 2ω. Finally, according to Ohm's law, the voltage variation at the tip end was a function of 3ω. Then the temperature increase could be express as

$$\Delta T_{2\omega} = \frac{2V_{3\omega}}{R_0 I_0 \alpha_R} \tag{3-40}$$

where, $V_{3\omega}$, R_0 and α_R are the third harmonic voltage, electrical resistance at ambient temperature and the temperature coefficient of the tip, respectively.

Therefore, a lock-in measurement of the 3ω output voltage gave insight on the temperature increase of the tip. When the tip contacted with the NW, the heat generated at the tip passed to the sample, and this flow depended on the thermal conductance of the sample (mid of Fig. 11(a)). In other words, the tip temperature variation $\Delta T_{2\omega}$ was related with the equivalent thermal resistance R_{eq} between the tip and the sample. Experimentally, the tip scaned the sample, and, then, the $\Delta T_{2\omega}$ tip temperature variation map and the equivalent tip-sample thermal resistance R_{eq} image could be obtained.[241]

From the equivalent thermal resistance values, the mean thermal conductivity of the NWs could be evaluated. Since the tip was on the top of the NW, the NW equivalent thermal resistance $(R_{eq})_{NW}$ was considered as four thermal resistances in series (shown at right side of Fig. 11(a)),

$$\left(R_{eq}\right)_{NW} = R_{Tip-NW} + R_c + R_{NW} + R_{NW-Sub} \tag{3-41}$$

where R_{Tip-NW}, R_{NW-Sub}, R_c and R_{NW} are the constriction resistance of the heat flux between the tip and the NW, the constriction resistance of the heat flux between the NW and the substrate, the tip-sample contact thermal resistance and the sample intrinsic thermal resistance, respectively.

Fortunately, R_{Tip-NW} was negligible since the thermal exchange surface was bigger than the NW section. Additionally, both R_{NW-Sub} and R_c could be estimated.[241,244] As a consequence, the mean NW thermal conductivity could be extracted from the intrinsic thermal resistance R_{NW},

$$\kappa_{NW} = \frac{1}{R_{NW}} \frac{l}{A_S} \tag{3-42}$$

where l and A_S are the length and cross section of the NW, respectively.

III-12.3 Merits and shortages

This method was able to thermally probe, with a thermal spatial resolution around 100 nm, a wide range of individual NWs embedded in a matrix and it took only a few minutes. Additionally, this method did not require pulling the NWs out from the matrix and suspending it. The intrinsic thermal conductivity of the sample, therefore,

RSC Advances Accepted Manuscript

could be obtained since it prevented the degradation of the NWs when exposed to air or dissolved in a solution. To obtain reliable thermal conductivities of the NWs, however, both the tip-sample thermal contact resistances, R_c, and the constriction resistance of the heat flux between the NW and the substrate, $R_{NW\text{-}Sub}$, deserved careful consideration. For instances, the tip-sample thermal contact resistance had been evaluated as 5.5×10^4 K/W which was comparable to the intrinsic thermal resistance of each imaged SiNW.[241] The R_c mostly depended on the experimental conditions, especially on the NW diameter and the thermal exchange diameter between the tip and sample.[245] New calibrations of these two resistances and the thermal probe were demanded for each new sample in order to obtain the thermal conductivities of the NWs accurately.

III-12.4 Applications

The mean thermal conductivity of individual Si NWs, with diameters ranging from 200 to 380 nm embedded in a matrix, as shown in Fig. 11(b), had been measured using SThM method within the 3ω mode by Puyoo et al..[241] Their SThM thermal imaging of Si NWs embedded in a silica matrix was in Fig. 11(c). However, from their results (Fig. 11(d)), no significant thermal conductivity of NWs was reduced compared with that of bulk Si. Muñoz Rojo et al.[244] had evaluated the mean thermal conductivity of Bi_2Te_3 NWs around 200 nm in diameter using SThM in a 3ω experimental configuration. The estimated mean thermal conductivity of the NWs was (1.37±0.20) W/mK, showing a slight thermal conductivity reduction. Recently, this method had also been successfully utilized to measure the mean thermal conductivity of SiGe NWs,[246] Sb_2Te_3 phase change NWs[245,246] and polymeric P3HT NWs.[247]

Ⅳ Prospect & Conclusions

In the past decades, various methods for measuring the 1D nanostructure thermoelectric properties had experienced remarkable developments. For practical application of thermoelectric material, further increasing accuracy and reliability of the measurement was still the main goal. Therefore, the difficulties of the measuring methods, such as the electrical and thermal contact resistances and the noises of the measurements, must be overcome before a universal thermoelectric device could be fabricated. Through papers reading, analysis and writing of this manuscript, to our knowledge, the following two topics in measuring the 1D nanostructure thermoelectric properties might be more and more active in the near future. The first involved utilizing specific suspended microstructures to access not only to the thermal conductivity but also to the Seebeck coefficient.[146-150] Hence, these microfabricated structures offered a route to obtain the figure of merits of the NWs. The second topic was using SThM in a 3ω experimental configuration.[241,244] In this setup, it did not require pulling the NW out from the matrix and suspending it so to prevent the surface modification of the NW. Therefore, the intrinsic thermal conductivity of the NW could be obtained.

In summary, a comprehensive revision of different methods to measure thermoelectric properties of 1D nanostructural materials have been presented. Five frequently used methods to measure the Seebeck coefficient have been reviewed. And twelve kinds of the most popular methods to measure the thermal conductivity have been discussed in details. In each method, its principle, applications, merits and shortages have been presented.

RSC Advances Accepted Manuscript

Two potential hot topics in measuring the 1D nanostructure thermoelectric properties have been proposed based on a large number of published papers.

Acknowledgments

The authors greatly acknowledge the support from the National Natural Science Foundation of China under grant numbers 61474115, 61404128, 61372059 and 61274066, and the National High Technology Research and Development Program of China (863 Program) under the grant number 2014AA032302.

References

1. L. E. Bell, *Science*, 2008, **321**, 1457-1461.
2. C. Wu, F. Feng and Y. Xie, *Chemical Society Reviews*, 2013, **42**, 5157-5183.
3. K. Singh, J. Nowotny and V. Thangadurai, *Chemical Society Reviews*, 2013, **42**, 1961-1972.
4. N. Linares, A. M. Silvestre-Albero, E. Serrano, J. Silvestre-Albero and J. Garcia-Martinez, *Chemical Society Reviews*, 2014, **43**, 7681-7717.
5. T. J. Seebeck, *Abhandlungen der Deustchen Akademi der Wissenschaften zu Berlin*, 1823, 265–373.
6. A. V. Shevelkov, *Dalton transactions*, 2010, **39**, 977-977.
7. J. H. Bahk, H. Y. Fang, K. Yazawa and A. Shakouri, *Journal of Materials Chemistry C*, 2015, **3**, 10362-10374.
8. P. Sundarraj, D. Maity, S. S. Roy and R. A. Taylor, *RSC Adv.*, 2014, **4**, 46860-46874.
9. J. Wei, Z. B. Nie, G. P. He, L. Hao, L. L. Zhao and Q. Zhang, *RSC Adv.*, 2014, **4**, 48128-48134.
10. L. L. Baranowski, G. J. Snyder and E. S. Toberer, *Energ Environ Sci*, 2012, **5**, 9055-9067.
11. Z. Wang, M. Kroener and P. Woias, *TRANSDUCERS 2011 - 2011 16th International Solid-State Sensors, Actuators and Microsystems Conference*, 2011, 1867-1870.
12. M. Arun, *Nat Nanotechnol*, 2009, **4**, 214-215.
13. I. Chowdhury, R. Prasher, K. Lofgreen, G. Chrysler, S. Narasimhan, R. Mahajan, D. Koester, R. Alley and R. Venkatasubramanian, *Nat Nanotechnol*, 2009, **4**, 235-238.
14. J. P. Heremans, M. S. Dresselhaus, L. E. Bell and D. T. Morelli, *Nat Nanotechnol*, 2013, **8**, 471-473.
15. L. D. Hicks and M. S. Dresselhaus, *Phys Rev B*, 1993, **47**, 16631-16634.
16. A. I. Boukai, Y. Bunimovich, J. Tahir-Kheli, J. K. Yu, W. A. Goddard, 3rd and J. R. Heath, *Nature*, 2008, **451**, 168-171.
17. A. I. Hochbaum and P. D. Yang, *Chemical Reviews*, 2010, **110**, 527-546.
18. V. Varshney, A. K. Roy, D. S. Dudis, J. Lee and B. L. Farmer, *Nanoscale*, 2012, **4**, 5009-5016.
19. W. Shi, S. Song and H. Zhang, *Chemical Society Reviews*, 2013, **42**, 5714-5743.
20. V. N. Popov, *Materials Science & Engineering R-Reports*, 2004, **43**, 61-102.
21. J. P. Small and P. Kim, *Microscale Thermophysical Engineering*, 2004, **8**, 1-5.
22. A. Druzhinin, I. Ostrovskii, I. Kogut, S. Nichkalo and T. Shkumbatyuk, *Phys. Status Solidi C*, 2011, **8**, 867–870.
23. N. B. Duarte, G. D. Mahan and S. Tadigadapa, *Nano Lett*, 2009, **9**, 617-622.
24. J. P. Feser, J. S. Sadhu, B. P. Azeredo, K. H. Hsu, J. Ma, J. Kim, M. Seong, N. X. Fang, X. Li, P. M. Ferreira, S. Sinha and D. G. Cahill, *Journal of Applied Physics*, 2012, **112**, 114306.

RSC Advances Accepted Manuscript

25. A. I. Hochbaum, R. Chen, R. D. Delgado, W. Liang, E. C. Garnett, M. Najarian, A. Majumdar and P. Yang, *Nature*, 2008, **451**, 163-167.
26. M. Jang, Y. Park, M. Jun, Y. Hyun, S. J. Choi and T. Zyung, *Nanoscale Res Lett*, 2010, **5**, 1654-1657.
27. F. Y. Ma, Y. Ou, Y. Yang, Y. M. Liu, S. H. Xie, J. F. Li, G. Z. Cao, R. Proksch and J. Y. Li, *J Phys Chem C*, 2010, **114**, 22038-22043.
28. J. Maire and M. Nomura, *Japanese Journal of Applied Physics*, 2014, **53**, 06JE09.
29. Y. Y. Qi, Z. Wang, M. L. Zhang, F. H. Yang and X. D. Wang, *J Phys Chem C*, 2013, **117**, 25090-25096.
30. J. W. Jiang, H. S. Park and T. Rabczuk, *Nanoscale*, 2013, **5**, 11035-11043.
31. G. G. Yadav, G. Zhang, B. Qiu, J. A. Susoreny, X. Ruan and Y. Wu, *Nanoscale*, 2011, **3**, 4078-4081.
32. F. J. DiSalvo, *Science*, 1999, **285**, 703-706.
33. P. Pichanusakorn and P. Bandaru, *Materials Science and Engineering: R: Reports*, 2010, **67**, 19-63.
34. C. Wang, Y. Wang, G. Zhang, C. Peng and G. Yang, *Physical Chemistry Chemical Physics*, 2014, **16**, 3771-3776.
35. J. Li, J. Sui, Y. Pei, X. Meng, D. Berardan, N. Dragoe, W. Cai and L.-D. Zhao, *J Mater Chem A*, 2014, **2**, 4903-4906.
36. W. Zhou, W. Zhao, Z. Lu, J. Zhu, S. Fan, J. Ma, H. H. Hng and Q. Yan, *Nanoscale*, 2012, **4**, 3926-3931.
37. G. Zhang and B. Li, *Nanoscale*, 2010, **2**, 1058-1068.
38. C. H. Will, M. T. Elm, P. J. Klar, B. Landschreiber, E. Güneş and S. Schlecht, *Journal of Applied Physics*, 2013, **114**, 193707.
39. Y. Liu, J. Lan, W. Xu, Y. Liu, Y.-L. Pei, B. Cheng, D.-B. Liu, Y.-H. Lin and L. D. Zhao, *Chemical Communications*, 2013, **49**, 8075-8077.
40. T. Zhang, J. Jiang, Y. Xiao, Y. Zhai, S. Yang and G. Xu, *J Mater Chem A*, 2013, **1**, 966-969.
41. A. Yusufu, K. Kurosaki, Y. Miyazaki, M. Ishimaru, A. Kosuga, Y. Ohishi, H. Muta and S. Yamanaka, *Nanoscale*, 2014, **6**, 13921-13927.
42. T. Souier, G. Li, S. Santos, M. Stefancich and M. Chiesa, *Nanoscale*, 2012, **4**, 600-606.
43. J. Liu, J. Sun and L. Gao, *Nanoscale*, 2011, **3**, 3616-3619.
44. Y. Jiang, Z. Wang, M. Shang, Z. Zhang and S. Zhang, *Nanoscale*, 2015, **7**, 10950-10953.
45. H. C. Chang, M. H. Chiang, T. C. Tsai, T. H. Chen, W. T. Whang and C. H. Chen, *Nanoscale*, 2014, **6**, 14280-14288.
46. H. T. Chang, S. Y. Wang and S. W. Lee, *Nanoscale*, 2014, **6**, 3593-3598.
47. S. Bathula, M. Jayasimhadri, B. Gahtori, N. K. Singh, K. Tyagi, A. K. Srivastava and A. Dhar, *Nanoscale*, 2015, **7**, 12474-12483.
48. K. Wang, H.-W. Liang, W.-T. Yao and S.-H. Yu, *J Mater Chem*, 2011, **21**, 15057-15062.
49. G. G. Yadav, A. David, T. Favaloro, H. Yang, A. Shakouri, J. Caruthers and Y. Wu, *J Mater Chem A*, 2013, **1**, 11901-11908.
50. E. O. Wrasse, A. Torres, R. J. Baierle, A. Fazzio and T. M. Schmidt, *Physical Chemistry Chemical Physics*, 2014, **16**, 8114-8118.
51. P. Vaqueiro and A. V. Powell, *J Mater Chem*, 2010, **20**, 9577-9584.
52. D. Liang, R. Ma, S. Jiao, G. Pang and S. Feng, *Nanoscale*, 2012, **4**, 6265-6268.
53. F. Zhou, A. L. Moore, J. Bolinsson, A. Persson, L. Froberg, M. T. Pettes, H. J. Kong, L. Rabenberg, P. Caroff, D. A. Stewart, N. Mingo, K. A. Dick, L. Samuelson, H. Linke and L. Shi, *Phys Rev B*, 2011, **83**, 205416.

RSC Advances Accepted Manuscript

54. X. Wang and Z. M. Wang, *Nanoscale Thermoelectrics,* Springer 2014, **16**.
55. J. R. Sootsman, D. Y. Chung and M. G. Kanatzidis, *Angewandte Chemie*, 2009, **48**, 8616-8639.
56. J. R. Szczech, J. M. Higgins and S. Jin, *J Mater Chem*, 2011, **21**, 4037-4055.
57. W. Liang, O. Rabin, A. I. Hochbaum, M. Fardy, M. Zhang and P. Yang, *Nano Research*, 2010, **2**, 394-399.
58. C. B. Vining, *Nature Materials*, 2009, **8**, 83-85.
59. K. F. Hsu, S. Loo, F. Guo, W. Chen, J. S. Dyck, C. Uher, T. Hogan, E. K. Polychroniadis and M. G. Kanatzidis, *Science*, 2004, **303**, 818-821.
60. T. C. Harman, P. J. Taylor, M. P. Walsh and B. E. LaForge, *Science*, 2002, **297**, 2229-2232.
61. R. Venkatasubramanian, E. Siivola, T. Colpitts and B. O'Quinn, *Nature*, 2001, **413**, 597-602.
62. K.-M. Lee, S.-K. Lee and T.-Y. Choi, *Applied Physics A*, 2011, **106**, 955-960.
63. G. Zhou, L. Li and G. H. Li, *Applied Physics Letters*, 2010, **97**, 023112.
64. L. Shi, D. Yao, G. Zhang and B. Li, *Applied Physics Letters*, 2010, **96**, 173108.
65. X. Zou, X. Chen, H. Huang, Y. Xu and W. Duan, *Nanoscale*, 2015, **7**, 8776-8781.
66. D. Demchenko, P. Heinz and B. Lee, *Nanoscale Research Letters*, 2011, **6**, 1-6.
67. Q. Zhang, T. Sun, F. Cao, M. Li, M. Hong, J. Yuan, Q. Yan, H. H. Hng, N. Wu and X. Liu, *Nanoscale*, 2010, **2**, 1256-1259.
68. G. Balasubramanian, I. K. Puri, M. C. Bohm and F. Leroy, *Nanoscale*, 2011, **3**, 3714-3720.
69. L. Lu, W. Yi and D. L. Zhang, *Rev Sci Instrum*, 2001, **72**, 2996-3003.
70. M. T. Demko, Z. Dai, H. Yan, W. P. King, M. Cakmak and A. R. Abramson, *Rev Sci Instrum*, 2009, **80**, 036103.
71. A. Weathers, K. Bi, M. T. Pettes and L. Shi, *Rev Sci Instrum*, 2013, **84**, 084903.
72. A. Boukai, K. Xu and J. R. Heath, *Advanced materials*, 2006, **18**, 864-869.
73. L. Shi, D. Li, C. Yu, W. Jang, D. Kim, Z. Yao, P. Kim and A. Majumdar, *Journal of Heat Transfer*, 2003, **125**, 881-888.
74. N. Akhtar and D. Vashaee, *2012 IEEE Green Technologies Conference*, 2012, 1-4.
75. G. G. Yadav, J. A. Susoreny, G. Zhang, H. Yang and Y. Wu, *Nanoscale*, 2011, **3**, 3555-3562.
76. A. Bulusu and D. G. Walker, *Superlattices and Microstructures*, 2008, **44**, 1-36.
77. Y. Y. Qi, Z. Wang, M. L. Zhang, F. H. Yang and X. D. Wang, *J Mater Chem A*, 2013, **1**, 6110-6124.
78. G. Pennelli, *Beilstein Journal of Nanotechnology*, 2014, **5**, 1268-1284.
79. S. B. Riffat and X. Ma, *Appl Therm Eng*, 2003, **23**, 913-935.
80. C. J. Vineis, A. Shakouri, A. Majumdar and M. G. Kanatzidis, *Advanced materials*, 2010, **22**, 3970-3980.
81. H. Younghoon, P. Youngsam, C. Wonchul, Z. Taehyoung and J. Moongyu, *Nanotechnology Materials and Devices Conference. IEEE*, 2011:194-195.
82. M. M. Rojo, O. C. Calero, A. F. Lopeandia, J. Rodriguez-Viejo and M. Martin-Gonzalez, *Nanoscale*, 2013, **5**, 11526-11544.
83. A. Weathers and L. Shi, *Annual Review of Heat Transfer*, 2013, **16**, 101-134.
84. C. H. Lee, G. C. Yi, Y. M. Zuev and P. Kim, *Applied Physics Letters*, 2009, **94**, 022106.
85. H. S. Shin, J. S. Lee, S. G. Jeon, J. Yu and J. Y. Song, *Measurement*, 2014, **51**, 470-475.
86. S. Karg, P. Mensch, B. Gotsmann, H. Schmid, P. Das Kanungo, H. Ghoneim, V. Schmidt, M. T. Bjork, V. Troncale and H. Riel, *J Electron Mater*, 2013, **42**, 2409-2414.
87. J. P. Small, L. Shi and P. Kim, *Solid State Communications*, 2003, **127**, 181-186.

RSC Advances Accepted Manuscript

88. B. C. Stephen, L. Yu-Ming, R. Oded, R. B. Marcie, Y. Y. Jackie, S. D. Mildred, L. G. Pratibha, M. Jean-Paul and I. Jean-Paul, *Nanotechnology*, 2002, **13**, 653-658.
89. A. Mavrokefalos, A. L. Moore, M. T. Pettes, S. Li, W. Wang and X. Li, *Journal of Applied Physics*, 2009, **105**, 104318.
90. L. A. Valentín, J. Betancourt, L. F. Fonseca, M. T. Pettes, L. Shi, M. Soszyński and A. Huczko, *Journal of Applied Physics*, 2013, **114**, 184301.
91. M. Murata and Y. Hasegawa, *Nanoscale Research Letters*, 2013, **8**, 400-410.
92. M. Murata, H. Yamamoto, F. Tsunemi, Y. Hasegawa and T. Komine, *J Electron Mater*, 2012, **41**, 1442-1449.
93. C. Guthy, C. Y. Nam and J. E. Fischer, *Journal of Applied Physics*, 2008, **103**, 064319.
94. E. Shapira, A. Tsukernik and Y. Selzer, *Nanotechnology*, 2007, **18**, 485703.
95. J. A. Martinez, P. P. Provencio, S. T. Picraux, J. P. Sullivan and B. S. Swartzentruber, *Journal of Applied Physics*, 2011, **110**, 074317.
96. J.-Y. Yu, S. W. Chung and J. R. Heath, *The Journal of Physical Chemistry B*, 2000, **104**, 11864-11870.
97. S. Y. Jang, H. S. Kim, J. Park, M. Jung, J. Kim, S. H. Lee, J. W. Roh and W. Lee, *Nanotechnology*, 2009, **20**, 415204.
98. Z. Wang, S. S. Adhikari, M. Kroener, D. Kojda, R. Mitdank, S. F. Fischer, W. Toellner, K. Nielsch, P. Woias and Ieee, in *26th Ieee International Conference on Micro Electro Mechanical Systems*, 2013, 508-511.
99. E. Z. Xu, Z. Li, J. A. Martinez, N. Sinitsyn, H. Htoon, N. Li, B. Swartzentruber, J. A. Hollingsworth, J. Wang and S. X. Zhang, *Nanoscale*, 2015, **7**, 2869-2876.
100. V. Schmidt, P. F. J. Mensch, S. F. Karg, B. Gotsmann, P. Das Kanungo, H. Schmid and H. Riel, *Applied Physics Letters*, 2014, **104**, 012113.
101. H. Younghoon, P. Youngsam, C. Wonchul, K. Jaehyeon, Z. Taehyoung and J. Moongyu, *Nanotechnology*, 2012, **23**, 405707.
102. J. Choi, K. Cho and S. Kim, *Microelectron Eng*, 2013, **111**, 126-129.
103. Y. M. Zuev, J. S. Lee, C. Galloy, H. Park and P. Kim, *Nano Letters*, 2010, **10**, 3037-3040.
104. P. Mensch, S. Karg, B. Gotsmann, P. Das Kanungo, V. Schmidt, V. Troncale, H. Schmid and H. Riel, *2013 43rd European Solid-State Device Research Conference (ESSDERC). Proceedings*, 2013, 252-255.
105. M. Noroozi, B. Hamawandi, M. S. Toprak and H. H. Radamson. *International Conference on Ultimate Integration on Silicon.* 2014, 125 - 128.
106. S. Jae Hun, A. L. Moore, S. K. Saha, Z. Feng, S. Li, Q. L. Ye, R. Scheffler, N. Mingo and T. Yamada, *Journal of Applied Physics*, 2007, **101**, 023706.
107. H. T. Huang, T. R. Ger, J. W. Chiang, Z. Y. Huang and M. F. Lai, *Ieee T Magn*, 2014, **50**, 1-4.
108. W. Xu, Y. Shi and H. Hadim, *Nanotechnology*, 2010, **21**, 395303.
109. C. Yu, S. Saha, J. Zhou, L. Shi, A. M. Cassell, B. A. Cruden, Q. Ngo and J. Li. *Journal of Heat Transfer,* 2006, **128**, 234-239.
110. D. Li, A. L. Prieto, W. Yiying, M. S. Martin-Gonzalez, A. Stacy, T. Sands, R. Gronsky, P. Yang and A. Majumdar, *21st International Conference on Thermoelectronics*, 2002, 333-336.
111. N. B. Duarte and S. A. Tadigadapa, *MEMS/MOEMS Components and Their Applications V. Special Focus Topics: Transducers at the Micro-Nano Interface.*, 2008, **6885**, 68850G.
112. S. F. Karg, V. Troncale, U. Drechsler, P. Mensch, P. Das Kanungo, H. Schmid, V. Schmidt, L. Gignac, H. Riel and B. Gotsmann, *Nanotechnology*, 2014, **25**, 305702.

RSC Advances Accepted Manuscript

113. E. K. Lee, L. Yin, Y. Lee, J. W. Lee, S. J. Lee, J. Lee, S. N. Cha, D. Whang, G. S. Hwang, K. Hippalgaonkar, A. Majumdar, C. Yu, B. L. Choi, J. M. Kim and K. Kim, *Nano Lett*, 2012, **12**, 2918-2923.
114. Y. Yang, D. K. Taggart, M. H. Cheng, J. C. Hemminger and R. M. Penner, *The Journal of Physical Chemistry Letters*, 2010, **1**, 3004-3011.
115. T. Ono, C. C. Fan and M. Esashi, *Journal of Micromechanics and Microengineering*, 2005, **15**, 1-5.
116. F. Völklein, H. Reith, M. C. Schmitt, M. Huth, M. Rauber and R. Neumann, *J Electron Mater*, 2009, **39**, 1950-1956.
117. S. B. Cronin, Y. M. Lin, M. R. Black, O. Rabin and M. S. Dresselhaus, *Xxi International Conference on Thermoelectrics, Proceedings Ict '02*, 2002, 243-248.
118. F. Volklein, M. Schmitt, T. W. Cornelius, O. Picht, S. Muller and R. Neumann, *J Electron Mater*, 2009, **38**, 1109-1115.
119. K. Kirihara, T. Sasaki, N. Koshizaki and K. Kimura, *Applied Physics Express*, 2011, **4**, 041201.
120. A. Potts, M. J. Kelly, D. G. Hasko, C. G. Smith, J. R. A. Cleaver, H. Ahmed, D. C. Peacock, D. A. Ritchie, J. E. F. Frost and G. A. C. Jones, *Microelectron Eng*, 1990, **11**, 15-18.
121. S. F. Svensson, A. I. Persson, E. A. Hoffmann, N. Nakpathomkun, H. A. Nilsson, H. Q. Xu, L. Samuelson and H. Linke, *New Journal of Physics*, 2012, **14**, 033041.
122. E. A. Hoffmann, H. A. Nilsson, L. Samuelson and H. Linke, *Physics of Semiconductors: 30th International Conference on the Physics of Semiconductors*, 2011, **1399**, 397-398.
123. J. Guo, X. Wang and T. Wang, *Journal of Applied Physics*, 2007, **101**, 063537.
124. J. Moon, K. Weaver, B. Feng, H. G. Chae, S. Kumar, J. B. Baek and G. P. Peterson, *Rev Sci Instrum*, 2012, **83**, 016103.
125. J. Q. Guo, X. W. Wang, D. B. Geohegan and G. Eres, *Functional Materials Letters*, 2008, **1**, 71-76.
126. N. K. Mahanta and A. R. Abramson, *Rev Sci Instrum*, 2012, **83**, 054904.
127. H. D. Wang, J. H. Liu, X. Zhang, R. F. Zhang and F. Wei, *Journal of Nanoscience & Nanotechnology*, 2015, **15**, 2939-2943.
128. M. C. Wingert, Z. C. Chen, E. Dechaumphai, J. Moon, J. H. Kim, J. Xiang and R. Chen, *Nano Lett*, 2011, **11**, 5507-5513.
129. P. Kim, L. Shi, A. Majumdar and P. McEuen, *Phys Rev Lett*, 2001, **87**, 215502.
130. J. Yang, Y. Yang, S. W. Waltermire, T. Gutu, A. A. Zinn, T. T. Xu, Y. Chen and D. Li, *Small*, 2011, **7**, 2334-2340.
131. M. T. Pettes and L. Shi, *Advanced Functional Materials*, 2009, **19**, 3918-3925.
132. H. Tang, X. Wang, Y. Xiong, Y. Zhao, Y. Zhang, Y. Zhang, J. Yang and D. Xu, *Nanoscale*, 2015, **7**, 6683-6690.
133. C. Yu, L. Shi, Z. Yao, D. Li and A. Majumdar, *Nano Letters*, 2005, **5**, 1842-1846.
134. S. Y. Lee, G. S. Kim, J. Lim, S. Han, B. W. Li, J. T. L. Thong, Y. G. Yoon and S. K. Lee, *Acta Materialia*, 2014, **64**, 62-71.
135. G. Yuan, R. Mitdank, A. Mogilatenko and S. F. Fischer, *J Phys Chem C*, 2012, **116**, 13767-13773.
136. A. L. Moore and L. Shi, *Measurement Science and Technology*, 2011, **22**, 015103.
137. L. D. Hicks and M. S. Dresselhaus, *Physical review. B, Condensed matter*, 1993, **47**, 12727-12731.
138. L. Shi, *Nanosc Microsc Therm*, 2012, **16**, 79-116.
139. M. S. Dresselhaus, G. Chen, M. Y. Tang, R. G. Yang, H. Lee, D. Z. Wang, Z. F. Ren, J. P. Fleurial and P. Gogna, *Advanced materials*, 2007, **19**, 1043-1053.

RSC Advances Accepted Manuscript

140. M. C. Wingert, Z. C. Chen, S. Kwon, J. Xiang and R. Chen, *Rev Sci Instrum*, 2012, **83**, 024901.
141. M. C. Wingert, J. Moon, Z. Chen, J. Xiang and R. K. Chen, *Proceedings of the Asme International Mechanical Engineering Congress and Exposition,* 2012, **11**, 385-391.
142. K. Davami, A. Weathers, N. Kheirabi, B. Mortazavi, M. T. Pettes, L. Shi, J. S. Lee and M. Meyyappan, *Journal of Applied Physics*, 2013, **114**, 134314.
143. M. Shaygan, N. Kheirabi, K. Davami, B. Mortazavi, J. S. Lee, G. Cuniberti and M. Meyyappan, *Materials Letters*, 2014, **135**, 87-91.
144. F. Zhou, A. Persson, L. Samuelson, H. Linke and L. Shi, *Applied Physics Letters*, 2011, **99**, 063110.
145. J. Zhu, K. Hippalgaonkar, S. Shen, K. Wang, Y. Abate, S. Lee, J. Wu, X. Yin, A. Majumdar and X. Zhang, *Nano Letters*, 2014, **14**, 4867-4872.
146. J. Zhou, C. Jin, J. H. Seol, X. Li and L. Shi, *Applied Physics Letters*, 2005, **87**, 133109.
147. H. Kim, Y. H. Park, I. Kim, J. Kim, H.J. Choi and W. Kim, *Applied Physics A*, 2011, **104**, 23-28.
148. S. C. Andrews, M. A. Fardy, M. C. Moore, S. Aloni, M. Zhang, V. Radmilovic and P. Yang, *Chemical Science*, 2011, **2**, 706-714.
149. K. Hippalgaonkar, B. Huang, R. Chen, K. Sawyer, P. Ercius and A. Majumdar, *Nano Letters*, 2010, **10**, 4341-4348.
150. Z. Guan, T. Gutu, J. K. Yang, Y. Yang, A. A. Zinn, D. Y. Li and T. T. Xu, *J Mater Chem*, 2012, **22**, 9853-9860.
151. C. L. Hsin, M. Wingert, C. W. Huang, H. Guo, T. J. Shih, J. Suh, K. Wang, J. Wu, W. W. Wu and R. Chen, *Nanoscale*, 2013, **5**, 4669-4672.
152. A. L. Moore, M. T. Pettes, F. Zhou and L. Shi, *Journal of Applied Physics*, 2009, **106**, 034310.
153. J. Kim, S. Lee, Y. M. Brovman, P. Kim and W. Lee, *Nanoscale*, 2015, **7**, 5053-5059.
154. H. S. Shin, S. G. Jeon, J. Yu, Y. S. Kim, H. M. Park and J. Y. Song, *Nanoscale*, 2014, **6**, 6158-6165.
155. J. E. Sale, M. Bemark, G. T. Williams, C. J. Jolly, M. R. Ehrenstein, C. Rada, C. Milstein and M. S. Neuberger, *Philosophical transactions of the Royal Society of London. Series B, Biological sciences*, 2001, **356**, 21-28.
156. J. W. Roh, S. Y. Jang, J. Kang, S. Lee, J. S. Noh, J. Park and W. Lee, *Korean J Met Mater*, 2010, **48**, 175-179.
157. A. Mavrokefalos, M. T. Pettes, S. Saha, Z. Feng and S. Li, *Thermoelectrics, 2006. ICT '06. 25th International Conference on*, 2006, 234 - 237.
158. O. Bourgeois, T. Fournier and J. Chaussy, *Journal of Applied Physics*, 2007, **101**, 016104.
159. S. W. Finefrock, Y. Wang, J. B. Ferguson, J. V. Ward, H. Fang, J. E. Pfluger, D. S. Dudis, X. Ruan and Y. Wu, *Nano Lett*, 2013, **13**, 5006-5012.
160. S. Y. Lee, M. R. Lee, N. W. Park, G. S. Kim, H. J. Choi, T. Y. Choi and S. K. Lee, *Nanotechnology*, 2013, **24**, 495202.
161. K. M. Lee, T. Y. Choi, S. K. Lee and D. Poulikakos, *Nanotechnology*, 2010, **21**, 125301.
162. S. Vollebregt, S. Banerjee, A. N. Chiaramonti, F. D. Tichelaar, K. Beenakker and R. Ishihara, *Journal of Applied Physics*, 2014, **116**, 023514.
163. H.-F. Lee, B. A. Samuel and M. A. Haque, *Journal of Thermal Analysis and Calorimetry*, 2009, **99**, 495-500.
164. C. Dames and G. Chen, *Rev Sci Instrum*, 2005, **76**, 124902.
165. J. Hou, X. Wang, P. Vellelacheruvu, J. Guo, C. Liu and H.-M. Cheng, *Journal of Applied Physics*, 2006, **100**, 124314.
166. O. M. Corbino, *Physikalische Zeitschrift*, 1910, **11**, 413-417.
167. D. G. Cahill, *Rev Sci Instrum*, 1990, **61**, 802.

RSC Advances Accepted Manuscript

168. D. G. Cahill and R. O. Pohl, *Phys Rev B*, 1987, **35**, 4067-4073.
169. S. M. Lee and S. I. Kwun, *Rev Sci Instrum*, 1994, **65**, 966-970.
170. I. K. Moon, Y. H. Jeong and S. I. Kwun, *Rev Sci Instrum*, 1996, **67**, 29-35.
171. L. R. Holland and R. C. Smith, *Journal of Applied Physics*, 1966, **37**, 4528-4536.
172. J. H. Kim, A. Feldman and D. Novotny, *Journal of Applied Physics*, 1999, **86**, 3959-3963.
173. C. E. Raudzis, F. Schatz and D. Wharam, *Journal of Applied Physics*, 2003, **93**, 6050-6055.
174. G. D. Li, D. Liang, R. L. J. Qiu and X. P. A. Gao, *Applied Physics Letters*, 2013, **102**, 043104.
175. H. Wang and M. Sen, *Int J Heat Mass Tran*, 2009, **52**, 2102-2109.
176. H. C. Chang, C. H. Chen and Y. K. Kuo, *Nanoscale*, 2013, **5**, 7017-7025.
177. D. Yang, C. Lu, H. Yin and I. P. Herman, *Nanoscale*, 2013, **5**, 7290-7296.
178. J. Lu, R. Guo, W. Dai and B. Huang, *Nanoscale*, 2015, **7**, 7331-7339.
179. S. T. Huxtable, A. R. Abramson, C. L. Tien, A. Majumdar, C. LaBounty, X. Fan, G. H. Zeng, J. E. Bowers, A. Shakouri and E. T. Croke, *Applied Physics Letters*, 2002, **80**, 1737-1739.
180. C. Zhen, J. Yang and Y. Chen, *IEEE International Conference on Nano/micro Engineered and Molecular Systems,* 2006, 283-286.
181. T. Y. Choi, M. H. Maneshian, B. Kang, W. S. Chang, C. S. Han and D. Poulikakos, *Nanotechnology*, 2009, **20**, 315706.
182. F. Chen, J. Shulman, Y. Xue, C. W. Chu and G. S. Nolas, *Rev Sci Instrum*, 2004, **75**, 4578-4584.
183. Y. Hasegawa, M. Murata, F. Tsunemi, Y. Saito, K. Shirota, T. Komine, C. Dames and J. E. Garay, *J Electron Mater*, 2013, **42**, 2048-2055.
184. J. Xie, A. Frachioni, D. S. Williams and B. E. White, Jr., *Applied Physics Letters*, 2013, **102**, 193101.
185. B. Hamdou, A. Beckstedt, J. Kimling, A. Dorn, L. Akinsinde, S. Bassler, E. Pippel and K. Nielsch, *Nanotechnology*, 2014, **25**, 365401.
186. L. Li, C. Jin, S. Xu, J. Yang, H. Du and G. Li, *Nanotechnology*, 2014, **25**, 415704.
187. S. Dhara, H. S. Solanki, A. R. Pawan, V. Singh, S. Sengupta, B. A. Chalke, A. Dhar, M. Gokhale, A. Bhattacharya and M. M. Deshmukh, *Phys Rev B*, 2011, **84**, 121307.
188. T. C. Hsiung, C. Y. Mou, T. K. Lee and Y. Y. Chen, *Nanoscale*, 2015, **7**, 518-523.
189. T. Y. Choi, D. Poulikakos, J. Tharian and U. Sennhauser, *Applied Physics Letters*, 2005, **87**, 013108.
190. T. Y. Choi, D. Poulikakos, J. Tharian and U. Sennhauser, *Nano Lett*, 2006, **6**, 1589-1593.
191. C. Xing, C. Jensen, T. Munro, B. White, H. Ban and M. Chirtoc, *Appl Therm Eng*, 2014, **73**, 317-324.
192. B. Feng, Z. X. Li, X. Zhang and G. P. Peterson, *Journal of Vacuum Science & Technology B*, 2009, **27**, 2280-2285.
193. C. Xing, C. Jensen, T. Munro, B. White, H. Ban and M. Chirtoc, *Appl Therm Eng*, 2014, **71**, 589-595.
194. P. C. Lee, H. C. Chen, C. M. Tseng, W. C. Lai, C. H. Lee, C. S. Chang and Y. Y. Chen, *Chinese J Phys*, 2013, **51**, 854-861.
195. M. Fujii, X. Zhang and K. Takahashi, *Physica Status Solidi B-Basic Solid State Physics*, 2006, **243**, 3385-3389.
196. X. Zhang, S. Fujiwara and M. Fujii, *International Journal of Thermophysics*, 2000, **21**, 965-980.
197. J. L. Wang, M. Gu, X. Zhang and Y. Song, *Journal of Physics D: Applied Physics*, 2009, **42**, 105502.
198. M. Fujii, X. Zhang, H. Xie, H. Ago, K. Takahashi, T. Ikuta, H. Abe and T. Shimizu, *Phys Rev Lett*, 2005, **95**, 065502.
199. Y. Ito, K. Takahashi, M. Fujii and X. Zhang, *Heat Transfer-Asian Research*, 2009, **38**, 297-312.

RSC Advances Accepted Manuscript

200. C. T. Harris, J. A. Martinez, E. A. Shaner, J. Y. Huang, B. S. Swartzentruber, J. P. Sullivan and G. Chen, *Nanotechnology*, 2011, **22**, 275308.
201. X. Zhang and J. L. Wang, *Proceedings of the Asme 9th International Conference on Nanochannels, Microchannels and Minichannels,* 2011, **2**, 707-712.
202. J. Wang and X. Zhang, *Japanese Journal of Applied Physics*, 2011, **50**, 11RC01.
203. C. Dames, S. Chen, C. T. Harris, J. Y. Huang, Z. F. Ren, M. S. Dresselhaus and G. Chen, *Rev Sci Instrum*, 2007, **78**, 104903.
204. M. F. P. Bifano, J. Park, P. B. Kaul, A. K. Roy and V. Prakash, *Journal of Applied Physics*, 2012, **111**, 054321.
205. A.-T. Chien, P. V. Gulgunje, H. G. Chae, A. S. Joshi, J. Moon, B. Feng, G. P. Peterson and S. Kumar, *Polymer*, 2013, **54**, 6210-6217.
206. J. B. Hou, X. W. Wang and J. Q. Guo, *Journal of Physics D-Applied Physics*, 2006, **39**, 3362-3370.
207. J. B. Hou, X. W. Wang and L. J. Zhang, *Applied Physics Letters*, 2006, **89**, 152504.
208. B. Feng, W. G. Ma, Z. X. Li and X. Zhang, *Rev Sci Instrum*, 2009, **80**, 064901.
209. J. Q. Guo, X. W. Wang, D. B. Geohegan, G. Eres and C. Vincent, *Journal of Applied Physics*, 2008, **103**, 113505.
210. J. W. Tan, Y. Cheng, D. S. G. Yap, F. Gong, S. T. Nguyen and H. M. Duong, *Chemical Physics Letters*, 2013, **555**, 239-246.
211. J. Guo, X. Wang, L. Zhang and T. Wang, *Applied Physics A*, 2007, **89**, 153-156.
212. X. Feng, X. Wang, X. Chen and Y. Yue, *Acta Materialia*, 2011, **59**, 1934-1944.
213. X. Feng and X. Wang, *Thin Solid Films*, 2011, **519**, 5700-5705.
214. X. Huang, J. Wang, G. Eres and X. Wang, *Carbon*, 2011, **49**, 1680-1691.
215. G. Liu, H. Lin, X. Tang, K. Bergler and X. Wang, *Journal of Visualized Experiments*, 2014, **83**, e51144.
216. F. Gong, Y. Cheng, J. W. Tan, S. G. D. Yap, S. T. Nguyen and H. M. Duong, *International Journal of Thermal Sciences*, 2014, **77**, 165-171.
217. C. Xing, T. Munro, C. Jensen and H. Ban, *Measurement Science and Technology*, 2013, **24**, 105603.
218. T. Wang, X. Wang, J. Guo, Z. Luo and K. Cen, *Applied Physics a-Materials Science & Processing*, 2007, **87**, 599-605.
219. Y. A. Yue, G. Eres, X. W. Wang and L. Y. Guo, *Applied Physics a-Materials Science & Processing*, 2009, **97**, 19-23.
220. Q. Li, C. Liu, X. Wang and S. Fan, *Nanotechnology*, 2009, **20**, 145702.
221. H. Scheel, S. Reich, A. C. Ferrari, M. Cantoro, A. Colli and C. Thomsen, *Applied Physics Letters*, 2006, **88**, 233114.
222. P. Puech, A. Anwar, E. Flahaut, D. Dunstan, A. Bassil and W. Bacsa, *Phys Rev B*, 2009, **79**, 085418.
223. J. Yang, S. Waltermire, Y. Chen, A. A. Zinn, T. T. Xu and D. Li, *Applied Physics Letters*, 2010, **96**, 023109.
224. J. Liu, H. Wang, W. Ma, X. Zhang and Y. Song, *Rev Sci Instrum*, 2013, **84**, 044901.
225. Y. Yue, X. Huang and X. Wang, *Physics Letters A*, 2010, **374**, 4144-4151.
226. M. Soini, I. Zardo, E. Uccelli, S. Funk, G. Koblmüller, A. Fontcuberta i Morral and G. Abstreiter, *Applied Physics Letters*, 2010, **97**, 263107.
227. Z. L. Wang, X. J. Chen, Q. Yan and J. Zhang, *Epl-Europhys Lett*, 2012, **100**, 14002.
228. G. S. Doerk, C. Carraro and R. Maboudian, *ACS Nano*, 2010, **4**, 4908-4914.

RSC Advances Accepted Manuscript

229. A. A. Balandin, S. Ghosh, W. Bao, I. Calizo, D. Teweldebrhan, F. Miao and C. N. Lau, *Nano Letters*, 2008, **8**, 902-907.
230. W. Cai, A. L. Moore, Y. Zhu, X. Li, S. Chen, L. Shi and R. S. Ruoff, *Nano Letters*, 2010, **10**, 1645-1651.
231. I. K. Hsu, R. Kumar, A. Bushmaker, S. B. Cronin, M. T. Pettes, L. Shi, T. Brintlinger, M. S. Fuhrer and J. Cumings, *Applied Physics Letters*, 2008, **92**, 063119.
232. H. D. Wang, J. H. Liu, X. Zhang and Y. Song, *Int J Heat Mass Tran*, 2014, **70**, 40-45.
233. Q. Y. Li and X. Zhang, *Thermochim Acta*, 2014, **581**, 26-31.
234. H. Yan, N. K. Mahanta, L. J. Majerus, A. R. Abramson and M. Cakmak, *Polymer Engineering & Science*, 2014, **54**, 977-983.
235. L. J. Majerus, *Application of the Thermal Flash Technique for Characterizing High Thermal Diffusivity Micro and Nanostructures*, Case Western Reserve University, 2009.
236. N. K. Mahanta, A. R. Abramson and J. Y. Howe, *Journal of Applied Physics*, 2013, **114**, 163528.
237. N. K. Mahanta and A. R. Abramson, *Proceedings of the ASME/JSME 2011 8th Thermal Engineering Joint Conference,* 2011, **3**, 181-187.
238. Y. Zhang, J. Christofferson, A. Shakouri, D. Y. Li, A. Majumdar, Y. Y. Wu, R. Fan and P. D. Yang, *Ieee Transactions on Nanotechnology*, 2006, **5**, 67-74.
239. J. Christofferson, D. Vashaee, A. Shakouri and P. Melese, *Metrology-based Control for Micro-Manufacturing*, 2001.
240. D. Y. Li, Y. Y. Wu, P. Kim, L. Shi, P. D. Yang and A. Majumdar, *Applied Physics Letters*, 2003, **83**, 2934-2936.
241. E. Puyoo, S. Grauby, J. M. Rampnoux, E. Rouviere and S. Dilhaire, *Journal of Applied Physics*, 2011, **109**, 024302.
242. S. p. Lefèvre and S. Volz, *Rev Sci Instrum*, 2005, **76**, 033701.
243. L. Shi, S. Plyasunov, A. Bachtold, P. L. McEuen and A. Majumdar, *Applied Physics Letters*, 2000, **77**, 4295.
244. M. Muñoz Rojo, S. Grauby, J. M. Rampnoux, O. Caballero-Calero, M. Martin-Gonzalez and S. Dilhaire, *Journal of Applied Physics*, 2013, **113**, 054308.
245. S. Grauby, E. Puyoo, J. M. Rampnoux, E. Rouviere and S. Dilhaire, *J Phys Chem C*, 2013, **117**, 9025-9034.
246. A. Saci, J. L. Battaglia, A. Kusiak, R. Fallica and M. Longo, *Applied Physics Letters*, 2014, **104**, 263103.
247. M. M. Rojo, J. Martin, S. Grauby, T. Borca-Tasciuc, S. Dilhaire and M. Martin-Gonzalez, *Nanoscale*, 2014, **6**, 7858–7865.

RSC Advances Accepted Manuscript

Graphic Abstract

Measuring methods for thermoelectric propriety of one-dimensional nanostructural materials

Yang Liu, Mingliang Zhang*, An Ji, Fuhua Yang, and Xiaodong Wang*

Measuring methods for Seebeck coefficient and thermal conductivity of 1D nanostructural materials were reviewed and structures, principles, merits and shortages, and examples of every methods were discussed in details.

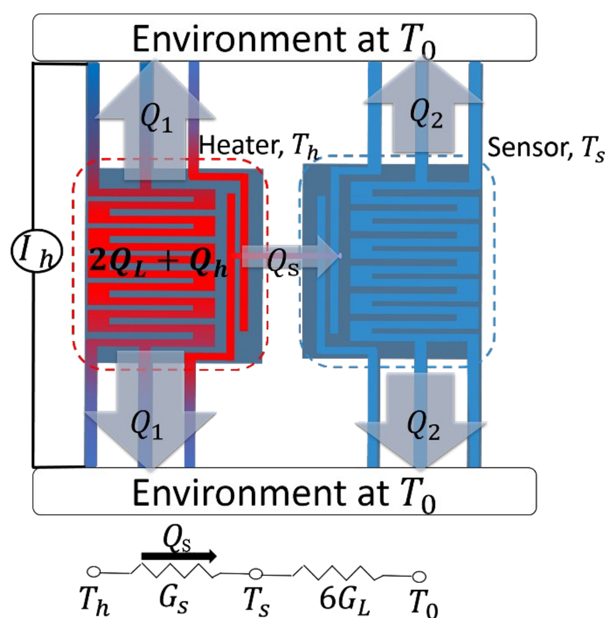

RSC Advances Accepted Manuscript